LEVEL II

NOSC

NOSC TR 336

AD A074461

NOSC TR 336

Technical Report 336

ECHO-ECHO CORRELATION

Comparative Study of Echo-Echo Correlation and Replica Correlation During the US/UK Joint Sonar Project Shows EEC to be a Superior Detection Process Under a Variety of Conditions

MD Green

15 August 1979

Final Report

Approved for public release; distribution unlimited.

NAVAL OCEAN SYSTEMS CENTER
SAN DIEGO, CALIFORNIA 92152

NAVAL OCEAN SYSTEMS CENTER, SAN DIEGO, CA 92152

AN ACTIVITY OF THE NAVAL MATERIAL COMMAND

SL GUILLE, CAPT, USN
Commander

HL BLOOD
Technical Director

ADMINISTRATIVE INFORMATION

The work reported on in this document was funded by the NOSC Independent Research Program (61152N, ZR78).

Released by
R. A. McLennan, Head
Sonar Systems Division

Under authority of
R. D. Thuleen, Head
Weapons Control and Sonar Department

ACKNOWLEDGMENTS

The author wishes to thank Dr. Jon Reeves and Darrell Marsh, both of NOSC, for their earlier work in this field and for their support and encouragement.

UNCLASSIFIED

SECURITY CLASSIFICATION OF THIS PAGE (When Data Entered)

REPORT DOCUMENTATION PAGE

READ INSTRUCTIONS BEFORE COMPLETING FORM

1. REPORT NUMBER: Technical Report 336 (NOSC TR 336)
2. GOVT ACCESSION NO.:
3. RECIPIENT'S CATALOG NUMBER:
4. TITLE (and Subtitle): ECHO-ECHO CORRELATION. Comparative Study of Echo-Echo Correlation and Replica Correlation During US/UK Joint Sonar Project Shows EEC to be a Superior Detection Process Under a Variety of Conditions. others
5. TYPE OF REPORT & PERIOD COVERED: Final Rep[redacted]
6. PERFORMING ORG. REPORT NUMBER:
7. AUTHOR(s): M D Green
8. CONTRACT OR GRANT NUMBER(s): 59
9. PERFORMING ORGANIZATION NAME AND ADDRESS: Naval Ocean Systems Center, San Diego, CA 92152
10. PROGRAM ELEMENT, PROJECT, TASK AREA & WORK UNIT NUMBERS: NOSC Independent Research 61152N (ZR78)
11. CONTROLLING OFFICE NAME AND ADDRESS: Naval Ocean Systems Center, San Diego, CA 92152
12. REPORT DATE: 15 Aug[redacted]79
13. NUMBER OF PAGES: 56
14. MONITORING AGENCY NAME & ADDRESS (if different from Controlling Office): NOSC/TR-336
15. SECURITY CLASS. (of this report): UNCLASSIFIED
15a. DECLASSIFICATION/DOWNGRADING SCHEDULE:
16. DISTRIBUTION STATEMENT (of this Report): Approved for public release; distribution unlimited
17. DISTRIBUTION STATEMENT (of the abstract entered in Block 20, if different from Report):
18. SUPPLEMENTARY NOTES:
19. KEY WORDS (Continue on reverse side if necessary and identify by block number): active sonar, signal processing, replica correlation, echo-echo correlation
20. ABSTRACT (Continue on reverse side if necessary and identify by block number):

This report provides a theoretical and computer-aided study into EEC signal processing and presents the results of EEC analysis on selected portions of data recorded during the US/UK Joint Sonar Project. A limited comparison with replica correlation analysis is also provided. Unique characteristics of the EEC process are identified and discussed, and its advantages over the RC process are suggested.

DD FORM 1473, 1 JAN 73 — EDITION OF 1 NOV 65 IS OBSOLETE

S/N 0102-LF-014-6601

UNCLASSIFIED

SECURITY CLASSIFICATION OF THIS PAGE (When Data Entered)

393 159

SUMMARY

In active sonar, large time-bandwidth product echoes from submerged objects are often identified through the use of a matched filter, or replica correlator. The theoretical characteristics of replica correlation (RC) are well known, but are predicated upon the echo being identical to the transmitted pulse, except for the presence of white Gaussian noise. When the ocean and target combine to filter the incident pulse in a random manner, the replica may no longer be a match for the echo.

Echo-Echo Correlation (EEC) is a method for exploiting the (assumed) stationarity of the medium and target to allow each echo in a train of three or more closely spaced echoes to be used as a match for the following echo. This results in a correlation technique that is insensitive to "echo splitting," target doppler, and pulse type. The sampled output of the correlator may be reduced by an almost arbitrary amount, thereby reducing the false alarm rate, but without affecting the probability of detection.

CONTENTS

INTRODUCTION . . . page 3

ECHO-ECHO CORRELATION . . . 4

SIGNAL-TO-NOISE RATIOS . . . 7

FALSE ALARMS . . . 8

COMPUTER SIMULATION . . . 10

COMPARISON OF ECHO DETECTABILITY . . . 13

EXPERIMENTS AT SEA . . . 16

Experimental Conditions . . . 16
Signal Processing . . . 17
Experimental Results . . . 17

CONCLUSIONS . . . 55

Location of Target Return . . . 55
Platform Stability . . . 55
Multipath and Echo Splitting Loss . . . 55
Target Doppler Sensitivity . . . 55
Pulse Type Sensitivity . . . 56
False Alarms . . . 56
SNR Enhancement . . . 56
Characteristic Appearance . . . 56

REFERENCES . . . 56

INTRODUCTION

The problem of detecting the presence of an underwater target began to receive attention during World War II as the danger from submarines and subsurface mines began to increase. In subsequent years the problem has expanded to include avoidance of submerged navigational obstacles such as wrecks and sea ice. The primary means now in use to detect these submerged dangers is sonar, which functions either by "listening" (passive reception) to the emitted sound of a target or by actively transmitting sound toward the target, then listening for the "echo," which is the reflection of the transmitted energy from the target. The echo will return to the receiver distorted to some degree by unwanted energy, which is called noise. The receiver system must contain some form of decision-making process which analyzes the returning energy with the goal of identifying, or detecting, the echo in the presence of the noise.

An echo returned from a perfect reflector will be identical to the transmitted pulse p(t), provided the medium through which the energy travels does not distort the wave. In the actual sonar environment, the target seldom acts as a perfect reflector, and the medium nearly always modifies the wave in several ways. A transmitted narrowband pulse of sound will be characterized by: its pulse length τ, its center frequency Ω, its bandwidth B ($B/\Omega \ll 1$), its initial phase ψ, and by its power. The parameters may be modified by the target and the medium in such a way that statistical estimation of each becomes necessary. When the range and/or the relative velocity of the target is unknown, the time of arrival of the echo may also have to be estimated.

When the echo is so buried in noise that its immediate identification is difficult, signal processing is required to extract the echo. The primary form of signal processing now in use with sonar, for narrowband pulses in which the product $B\tau$ is much greater than 1, is called Replica Correlation (RC). When the spectral density of the noise n(t), is also a narrowband function centered on Ω, the received time function will be

$$\begin{aligned} z(t) &= p(t) + n(t) \\ &= R\ell[Z(t)\exp(i\Omega t)] \qquad (1) \\ &= R\ell[(P(t)e^{i\psi} + N(t))\exp(i\Omega t)] \end{aligned}$$

where

Z(t), P(t), and N(t) are the complex envelopes (Ref. (1)) of z(t), p(t), and n(t), respectively.

The observation period of v(t) is $T \gg \tau$. Assume the data are sampled according to the Shannon sampling rule, at h samples per second. Replica correlation is defined as

$$\begin{aligned} r(\lambda) &= \frac{1}{hT} \sum_{j=0}^{hT} p(j+\lambda)\, z(j) \\ &= \frac{1}{hT} R\ell \left[\sum_{j=0}^{hT} e^{-i\psi} P^*(j+\lambda)\, Z(j) \right] \qquad (2) \end{aligned}$$

in which p(j), a replica of the transmitted pulse, is the optimum form of the matched filter for white noise. The time, λmax, of the largest amplitude of $r(\lambda)$ is taken as an estimate of the time of arrival of the echo.

Replica correlation presupposes that the echo is identical to the transmitted signal save for the effects of noise. The medium and target will often combine to filter the transmitted signal in such a way that the received echo no longer duplicates the replica. In general, it is not possible to predict the characteristics of this "external filter," and means are required to compensate for its effects, although the techniques employed with replica correlation have not been notably successful when severe distortion of the pulse occurs. The remainder of this paper presents a technique that eliminates the problems caused by the external filter.

ECHO-ECHO CORRELATION

If the external filter is fairly stationary over a period of several pulse lengths, it is possible to compensate for the pulse distortion by transmitting three or more closely spaced pulses, identifying one of the returning echoes, and using it as a "replica" for the remaining pulses. Let the transmitted signal be a series of pulses

$$a(t) = \sum_{m=1}^{M} p(t - mL) \tag{3}$$

where $L \geqslant \tau$ is the pulse repetition period,

$M \geqslant 3$ is the number of pulses,

and

$ML \ll T$.

The received sampled time function from a stationary target now is x(j), where

$$x(j) = b(j) + n(j) \quad , \qquad 0 \leqslant j \leqslant hT \tag{4}$$

where

$$b(j) = \sum_{m=1}^{M} q(j - mL)$$

q(j) is the received echo from one transmitted pulse, p(j).

At any time j_o, begin observing x(j) in segments each hL samples long. Let x_k be the k^{th} segment. Define Echo-Echo Correlation (EEC) as

$$c_k(\lambda) = \frac{1}{L}\left(\frac{L}{L-|\lambda|}\right)\sum_{j=0}^{(hL-|\lambda|)} x_k(j+\lambda)\, x_{k+1}(j)$$

$$= \frac{1}{L}\left(\frac{L}{L-|\lambda|}\right) R\ell \left[\sum_{j=0}^{hL-|\lambda|} X_k^*(j+\lambda)\, X_{k+1}(j)\right] \qquad (5)$$

$$-hL \leqslant \lambda \leqslant hL$$

where $X_k(j)$ is the complex envelope of $x_k(j)$.

There are two cases to be considered. First, assume that each individual echo, $q_\ell(j)$, $\ell = 1, 2, 3$, is wholly contained within the adjacent segment, $x_{k+\ell-1}(j)$. Refer to Fig. 1, where the

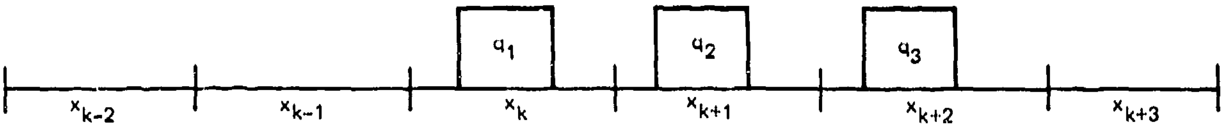

Figure 1

envelope of $x(j)$ is shown; the noise is suppressed. Assume that the first echo, $q_1(j)$, is contained in segment x_k, that the individual echoes q_ℓ are identical, although they may no longer resemble $p(j)$, and that the noise in each segment, $n_k(j)$, is statistically independent from signal and from noise in adjacent segments. Eq. (5) is used to obtain sample correlations of adjacent segments. There are seven input segments, which provide six correlation segments. They are

$$E[c_{k-2}(\lambda)] = \frac{1}{J}\sum_{j=0}^{J} E\{n_{k-2}(j+\lambda)\, n_{k-1}(j)\} = 0 \qquad (6)$$

where E is the expectation over the noise distribution,

$$J = (hL - |\lambda|) \ ,$$

$$E[c_{k-1}(\lambda)] = \frac{1}{J}\sum_{j=0}^{J} E\{n_{k-1}(j+\lambda)\, [q_1(j) + n_k(j)]\} = 0 \qquad (7)$$

$$E[c_k(\lambda)] = \frac{1}{J}\sum_{j=0}^{J} E\{[q_1(t+\lambda) + n_k(t+\lambda)]\, [q_2(t) + n_{k+1}(t)]\}\, dt$$

$$= \frac{1}{J}\sum_{j=0}^{J} q_1(t+\lambda)\, q_2(t)\, dt \qquad (8)$$

$$E[c_{k+1}(\lambda)] = \frac{1}{J} \sum_{j=0}^{J} E\{[q_2(j+\lambda) + n_{k+1}(j+\lambda)]\ [q_3(j) + n_{k+2}(j)]\}$$

$$= \frac{1}{J} \sum_{j=0}^{J} q_2(j+\lambda)\, q_3(j) \tag{9}$$

$$E[c_{k+2}(\lambda)] = \frac{1}{J} \sum_{j=0}^{J} E\{[q_3(j+\lambda) + n_{k+2}(j+\lambda)]\ n_{k+3}(j)\} = 0 \tag{10}$$

$$E[c_{k+3}(\lambda)] = \frac{1}{J} \sum_{j=0}^{J} E\{n_{k+3}(j+\lambda)\, n_{k+4}(j)\} = 0\,. \tag{11}$$

Note that noise correlated with noise [Eqs. (6), (11)] gives zero correlation, as does echo correlated with noise [Eqs. (7), (10)], while echo plus noise correlated with echo plus noise gives the autocorrelation of the echo [Eqs. (8), (9)]. Each correlation segment is 2L sec long.

In the second, and more general, case, each echo will be split between segments, as shown in Fig. 2. Note that $x_k(j)$ contains a portion of q_1, while $x_{k+1}(j)$ contains portions

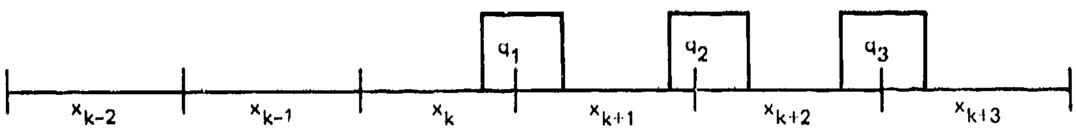

Figure 2

of both q_1 and q_2, etc. As before Eqs. (6), (7), and (11) show $E[c_{k-2}] = E[c_{k+1}] = E[c_{k+3}] = 0$. However, since $x_k(j)$ contains a part of $q_1(j)$ which is identical to the similar part of $q_2(j)$ in $x_{k+1}(j)$, $E[c_k]$ will be a partial autocorrelation. Segment $x_{k+1}(j)$ contains a complete echo (although the parts are rearranged) as does segment $x_{k+2}(j)$. Thus $E[c_{k+1}(\lambda)]$ follows Eq. (9), and produces a full autocorrelation. $E[c_{k+2}(\lambda)]$ again produces a partial autocorrelation. Since one of the two cases will always occur for a fixed target, Eq. (5) will always produce a full autocorrelation function for at least one value of k.

With both RC and EEC, the passage through the correlator of a sufficiently strong echo will result in a "peak" in the output which exceeds in amplitude the surrounding background caused by noise passing through the correlator. When no prior knowledge of the target's location is known, the output of the replica correlator must be computed for every value of λ to determine which $r(\lambda)$ is largest in magnitude. For EEC, on the other hand, Fig. 1 and Eq. (8) show that the peak must occur at the center of the output segment, $\lambda=0$, for a fixed target. Thus all values of $c_k(\lambda)$, for $\lambda \neq 0$ and all k, need not be computed. The reduction in computation over RC is apparent.

When the target moves with constant velocity relative to the transmitter/receiver, the effect is to change the pulse repetition period, L. If v is the relative target velocity, and V the speed of sound, then L′ is the echo repetition period,

$$L' = L\left(1 + \frac{2v}{V}\right) . \tag{12}$$

The individual echoes, $q_\ell(j)$, are each frequency shifted relative to the transmitted pulse, but not relative to each other. Since v is unknown, it must be estimated; however, since $v = (L'/L - 1)V/2$, L′ determines v. If information about the target's maximum speed is available, then the difference $|L-L'| \leqslant \delta$. Thus it becomes necessary to evaluate $c_k(\lambda)$ only for $|\lambda| \leqslant \delta$, and the time $\lambda_{max} \neq 0$ will thus determine (L–L′), hence L′ and v.

SIGNAL-TO-NOISE RATIOS

One of the primary measures of the effectiveness of a signal processing technique is its ability to improve the signal-to-noise ratio of the input z(j). Define the input signal-to-noise ratio as

$$S_i = F/\sigma_n^2 \tag{13}$$

where

F is the mean square amplitude of the echo, q(j), and σ_n^2 is the variance of n(j).

The output signal-to-noise ratio for RC [Eq. (2)] is

$$\begin{aligned} S_0 &= \{E[r(\lambda_{max})]\}^2/\sigma_r^2 \\ &\approx 2B\tau(S_i) \end{aligned} \tag{14}$$

where

σ_r^2 is the variance of r(λ)

and for EEC [Eq. (5)] it is

$$\begin{aligned} S_0 &= \{E[c_k(0)]\}^2/\sigma_{c_{k+2}}^2 \\ &\approx 2B\tau(S_i)^2 \end{aligned} \tag{15}$$

where

$\sigma_{c_{k+2}}^2$ is the variance of $c_{k+2}(\lambda)$.

The derivations of these formulas are given in Ref. 2.

It is interesting to note that, because the EEC peak occurs at $\lambda_{max} = 0$, for a target which is fixed relative to the receiver, the S_0 predicted by Eq. (15) can be doubled. Let

$$\bar{c}_k(\lambda) = \frac{1}{2}[c_k(\lambda) + c_k(-\lambda)] . \tag{16}$$

Define the new output signal-to-noise ratio to be

$$\bar{S}_0 = E[\bar{c}_k(0)] / \bar{\sigma}_1^2 \tag{17}$$

where

$$\bar{\sigma}_1^2 = \text{var}(\bar{c}_{k+2}(\lambda)) .$$

Now

$$E[\bar{c}_k(0)] = \frac{1}{2} E[c_k(0) + c_k(0)] = E[c_k(0)] ,$$

so that the signal part of $\bar{S}_0$ is unchanged from that of S_0. The noise variance is reduced by a factor of two, however, since

$$\begin{aligned} \bar{\sigma}_1^2 &= \frac{1}{4} \text{var} [c_{k+2}(\lambda) + c_{k+2}(-\lambda)] \\ &= \frac{1}{4} [\text{va. } c_{k+2}(\lambda) + \text{var } c_{k+2}(-\lambda)] \\ &= \frac{1}{4} [2 \text{ var } c_{k+2}(\lambda)] . \\ &= \frac{1}{2} \left(\sigma_{c_{k+2}}(\lambda)\right) . \end{aligned} \tag{18}$$

Since, for $\lambda \neq 0$, $c_{k+2}(\lambda)$ and $c_{k+2}(-\lambda)$ have independent white Gaussian noise, one has

$$\bar{S}_0 = 2S_0 . \tag{19}$$

In the remainder of the paper, the use of $\bar{c}_k(\lambda)$ will be referred to as the enhanced EEC technique.

FALSE ALARMS

A processor decides that an echo is present when the output is sufficiently high. The decision level D is often determined as a function of one or more of the noise statistics, so that, when noise alone enters a correlator, the possibility exists that the output will exceed the threshold. When this occurs, the results are interpreted as a false alarm.

For $B\tau \gg 1$, the Central Limit Theorem (Ref. 3) ensures that the probability density function (pdf) of the correlation of the noise will be Gaussian, both for RC [Eq. (2)] and EEC [Eq. (5), (16)] However, in the estimation of sonar parameters, it is often the case that the phase, ψ, and carrier frequency. Ω, are unimportant. Since the time functions of interest are narrowband, the phase and carrier of the echo envelope can be eliminated by computing the magnitude of the complex functions [Eq. (2), (5), and (16)]. Thus

$$\phi(\lambda) = |r(\lambda)| \text{ , for RC}$$

$$\rho_k(\lambda) = |c_k(\lambda)| \text{ , for EEC} \tag{20}$$

$$\alpha_k(\lambda) = |\bar{c}_k(\lambda)| \text{ for enhanced EEC.}$$

These are the correlation "envelopes," which will follow the Rayleigh distribution (Ref. 4) so that the probability of a false alarm, PFA, is, for RC

$$\text{PFA}(\phi > D_1) = \int_{D_1}^{\infty} \frac{\phi}{\sigma_{n_1}^2} \exp\left(\frac{-\phi^2}{2\sigma_{n_1}^2}\right) d\phi$$

$$= \exp\left(-D_1^2/2\sigma_{n_1}^2\right) \tag{21}$$

and for EEC

$$\text{PFA}(\rho_k > D_2) = \exp\left(-D_2^2/2\sigma_{n_2}^2\right) \tag{22}$$

$$\text{PFA}(\alpha_k > D_3) = \exp\left(-D_3^2/4\sigma_{n_2}^2\right) \tag{23}$$

where

D_i, i=1,2,3 is the respective threshold

$\sigma_{n_i}^2$, i=1,2 is the respective noise variance.

By forming a ratio of Eqs. (22) and (23), and setting $D_3 = D_2$, one has

$$\exp\left(-D_2^2/4\sigma_{n_2}^2\right) < 1 \tag{24}$$

for

$$D_2 > 0 \text{ ,}$$

which shows that using $\alpha_k(\lambda)$ in place of $\rho_k(\tau)$ will always give a reduced PFA for a given threshold level. On the other hand, if PFA in Eqs. (22) and (23) are equal, then $D_3 = D_2/\sqrt{2}$, so that the same result is obtained with a lower threshold for the enhanced technique.

It was previously mentioned that one need compute $c_k(\lambda)$ and/or $\bar{c}_k(\lambda)$, hence $\rho_k(\tau)$ and/or $\alpha_k(\lambda)$, only within some range, $-\delta \leqslant \lambda \leqslant \delta$. By not computing the correlation for $|\lambda| > \delta$, the opportunity for noise only output to exceed the threshold is reduced. Let

$$\gamma = \frac{2\delta}{2L} = \frac{\delta}{L} \tag{25}$$

which is seen to be a ratio between the necessary output duration, 2δ, and the maximum duration, 2L. The probability of a false alarm is thus reduced by the factor γ.

COMPUTER SIMULATION

One method for checking the validity of assumptions made in deriving theoretical equations is to make measurements on computer simulated data and to compare these results with the theoretical predictions. To that end, a pulse was generated and added to bandlimited white Gaussian noise. This input time function was used as $z(t)$ from Eq. (1) and was passed through both the replica correlator and the Echo-Echo Correlator. The output was observed, and the signal-to-noise ratio $\hat{S}_o$, measured. When $B\tau \gg 1$, the output of the correlator will be Gaussian, so that $\hat{S}_o$ may be computed from

$$\hat{S}_o = \left(\frac{F - \bar{Y}}{\sigma}\right)^2 \tag{26}$$

where

F is the peak of the correlation output when pulse (plus noise) has passed through the correlator $\bar{Y}$ is the sample mean of the output noise, σ is the sample variance of the output noise.

Equation (26) compares with Eqs. (14) and (15) when $\bar{Y} = 0$. When the envelopes of zero mean Gaussian correlator outputs (Eqs. (20)) are considered, a more appropriate measure to use is (Ref. 5)

$$\hat{S}_o = \left(\frac{F}{\bar{Y}\sqrt{2/\pi}}\right)^2 \tag{27}$$

where

F and Y are as before.

When S_i is computed as the mean square pulse amplitude divided by the noise variance, Eq. (27) is an asymptotically unbiased estimate of S_o as predicted by Eq. (14) or (15) as appropriate.

The pdf of the noise output can be estimated by computing a histogram of the data and comparing it with a theoretica[illegible] say by a "chi-squared Goodness of Fit Test" (Ref. 6). This estimate can be imp[illegible] averaging together several histograms of independent data. The mean, $\bar{Y}$, and va[illegible]e, $\bar{\sigma}^2$, of the data are estimated as

$$\hat{Y} = \frac{1}{MM} \sum_{\lambda=1}^{MM} Y(\lambda) \tag{28}$$

and

$$\hat{\sigma}^2 = \frac{1}{MM-1} \sum_{\lambda=1}^{MM} (Y(\lambda) - \hat{Y})^2 \tag{29}$$

where MM $\gg$ ht and $Y(\lambda)$ are samples of $\phi(\lambda)$, $\rho_k(\lambda)$, or $\alpha_k(\lambda)$, as appropriate. The False Alarm Rate K is estimated by counting the number of times in the observation period, T, that the noise only portion of the correlation exceeds a threshold, D. This threshold is usually a multiple of the output sample noise standard deviation, $\overline{\sigma}$.

The waveforms used in the sea trials were either Linear Period Modulated (LPM) pulses, or Pseudo Random Noise (PRN) pulses. See Reference 7 for a discussion of LPM signals. A set of three identically generated LPM pulses were generated in the computer and imbedded in bandlimited white noise. The pulse bandwidth was 15-70 Hz, and the pulse length, τ, was 0.853 sec. The pulse repetition period, L, was 1.333 sec. The noise bandwidth, to the 3-dB points, was approximately 15-70 Hz. See Figure 3, which represents the case in which each echo is wholly contained in a segment, $x_k(t)$ (Fig. 1). Equation (20) was evaluated from these data with results as shown in Figs. 4 and 5, for RC and EEC,

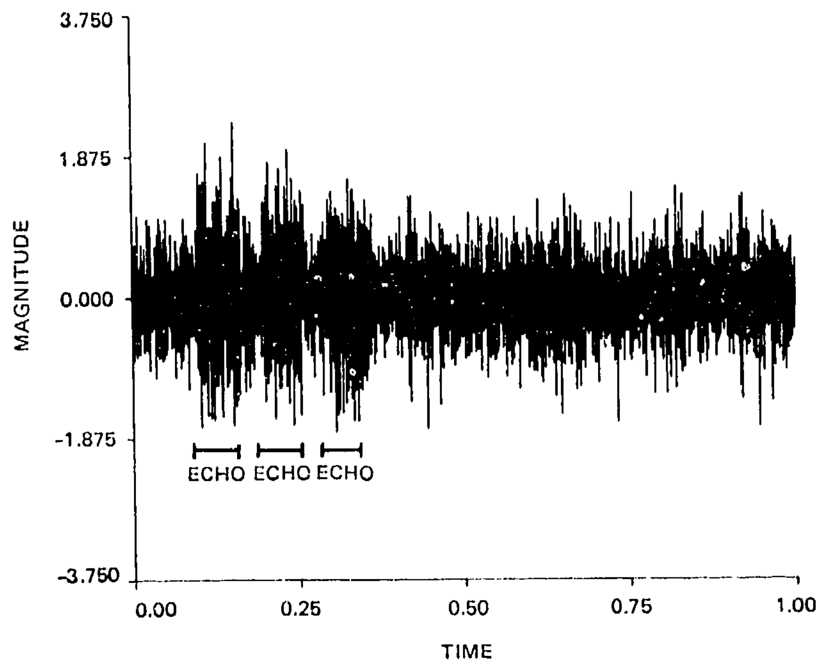

Figure 3. Computer simulated x(t) [Ref. Eq. (4)].

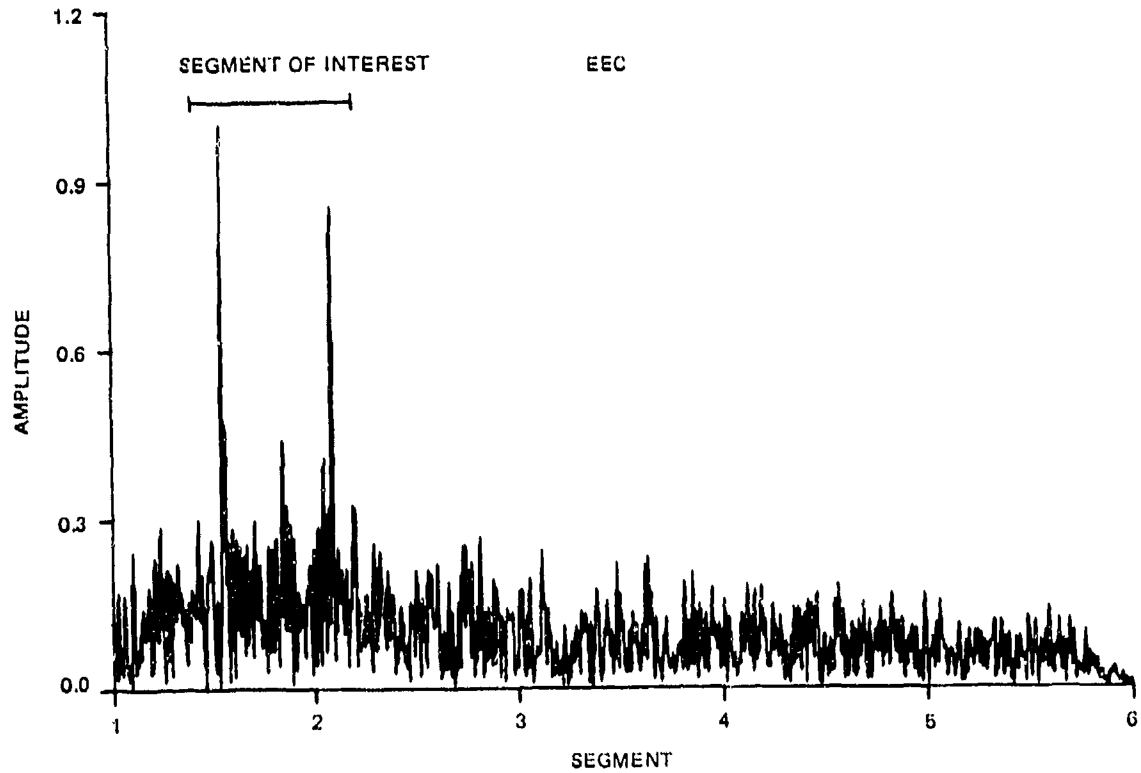

Figure 4. EEC output.

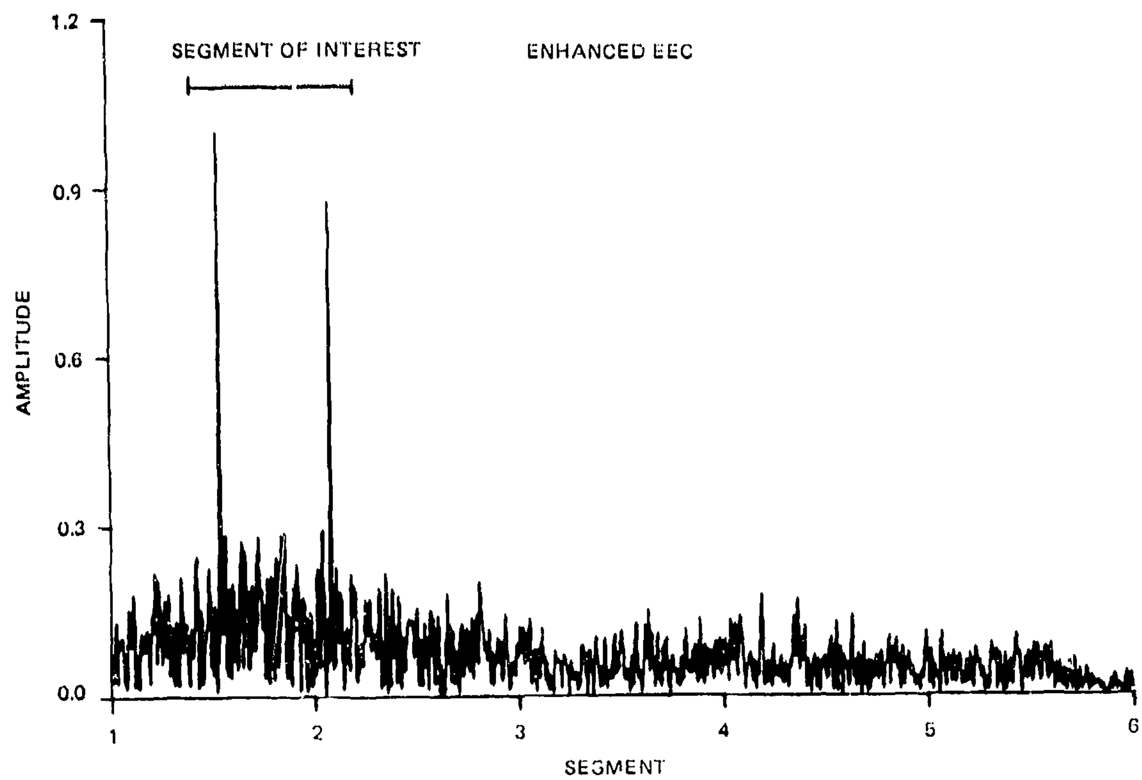

Figure 5. Enhanced EEC output.

respectively. Ten trials using the same pulse train mixed with independent noise samples were conducted and the results averaged. The input signal-to-noise ratio S_i, calculated as the mean square pulse amplitude divided by the input noise variance, was 2.85 dB, and the average output signal-to-noise ratio S_O, calculated by Eq. (27), was 22.36 ± 0.90 dB for $\rho_k(i)$, and 25.14 ± 0.8 dB for $\alpha_k(j)$. The predicted S_O, using Eq. (15), was 23.1 dB. A similar test was conducted for a case of arbitrarily located echoes (with respect to segment orientation – Fig. 2), with results very nearly the same as just described. Figure 6 shows a plot of the probability of false alarms exceeding a threshold, D, versus the threshold, given as fractions of the output mean, – Eq. (28). Note that the measured data points fit the theoretical curves very closely.

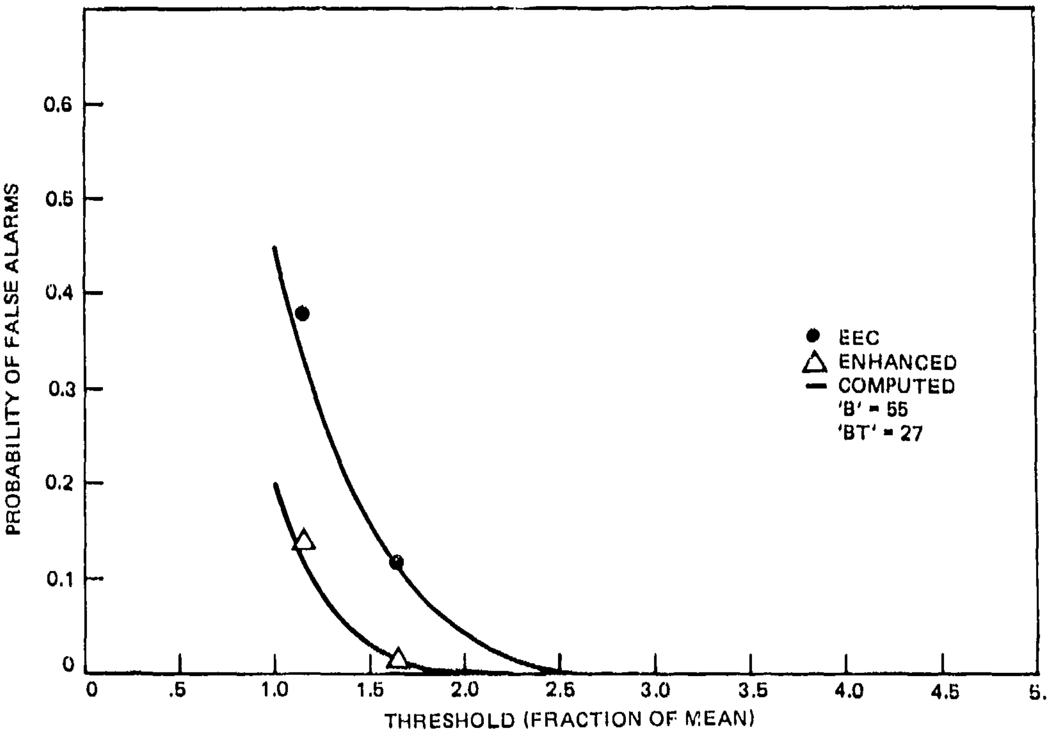

Figure 6. Probability of false alarms.

COMPARISON OF ECHO DETECTABILITY

The relative ability of two signal processing techniques to extract a recognizable echo from noise is a measure of the efficiency of one technique versus the other. The following comparison method is due to Brown (Ref. 2, pp 2–30), with modifications to suit the more restricted nature of this inquiry.

Define the False Alarm Rate, K, to be the number of false alarms which occur in some unit of time, and assign K to both techniques. Determine the S_i necessary for each technique to attain this K for a 50% probability of detection. For $B\tau \gg 1$, an acceptable estimate of K is

$$\hat{K} = PFA \cdot B \ . \tag{30}$$

Using Eqs. (24), (25), and (26), we have

$$K = PFA(\phi > D_1) \cdot B_1 = PFA(\rho > D_2) \cdot B_2 = PFA(\alpha > D_3) \cdot B_2 \tag{31}$$

where

B_i is i = 1, 2 bandwidth.

Solving Eq. (32) for D_i, we obtain

$$D_1 = \left(-2\,\sigma_{n1}^2\,\ell n\,(\hat{K})/B_1\right)^{1/2}$$

$$D_2 = \left(-2\,\sigma_{n2}^2\,\ell n\,(\hat{K})/B_2\right)^{1/2}$$

$$D_3 = \left(-4\,\sigma_{n2}^2\,\ell n\,(\hat{K})/B_2\right)^{1/2} = \sqrt{2}\,D_2 \ . \tag{32}$$

The mean, $\bar{Y}_R$ and the variance σ_R^2, of the Rayleigh distributed noise out of the correlator/detector is related to the variance, σ_n^2, of the input noise, n(t) [Eq. (1)] by the following (Ref. 5):

$$\bar{Y}_R = \sigma_n\sqrt{\pi/2},\ \sigma_R = \left(\frac{4-\pi}{2}\right)^{1/2}\sigma_n = \beta\,\sigma_n \ . \tag{33}$$

An "effective signal-to-noise ratio," d_i, is given for each technique as

$$\begin{aligned} d_i &= 20\log\left[(D_i - \bar{x}_{Ri})/\sigma_{Ri}\right] \\ &= 20\log\left[(D_i - \sigma_{ni}\sqrt{\pi/2})/\beta\sigma_{ni}\right] \ . \end{aligned} \tag{34}$$

Equation (34) is equivalent to Eq. (26). In order to determine S_i from Eq. (14) or (15), it is first necessary to compute $\hat{S}_0$ from Eq. (27), which is not linearly related to d_i. The non-linearity may be removed by application of (modified) Brown's curves, thus transforming d_i to an estimate of S_0 comparable to that obtained from Eq. (27).

As a numerical example, let $\sigma_{n1} = \sigma_{n2} = 1.0$, $B_1 = B_2 = B = 400$ Hz, $\tau = 1$ sec, so 10 log $(2B\tau)$ = 29 dB, and let K = 10^{-2} false alarms per sec. Thus, from Eqs. (22), (23) and (24)

$$D_1 = D_2 = 4.61$$

$$D_3 = 6.51$$

and from Eq. (34)

$$d_1 = d_2 = d_3 = 14.21 \text{ dB} \ .$$

From Fig. 7 we obtain, for RC, S_i = 12–29 = –17 dB, while from Fig. 8, for EEC, S_i = 6.5–14.5 = –8.5 dB, and for the enhanced EEC [Eq. (16)], S_i = 5.5–14.5 = –9.5 dB.

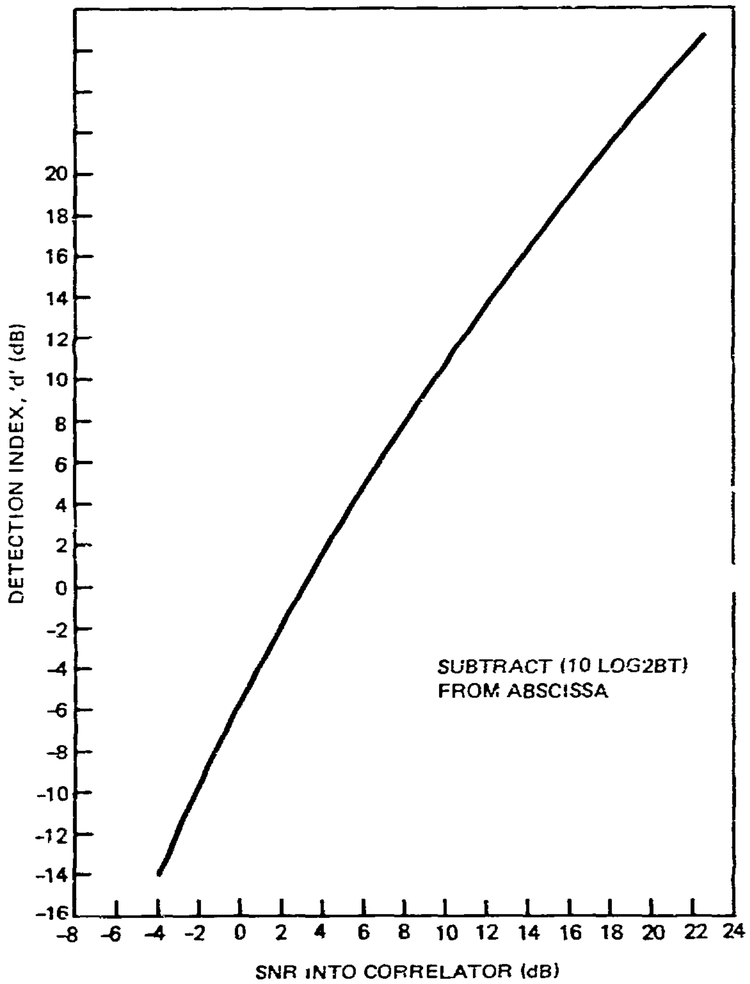

Figure 7. Detector output correlator input SNR transfer, replica correlator.

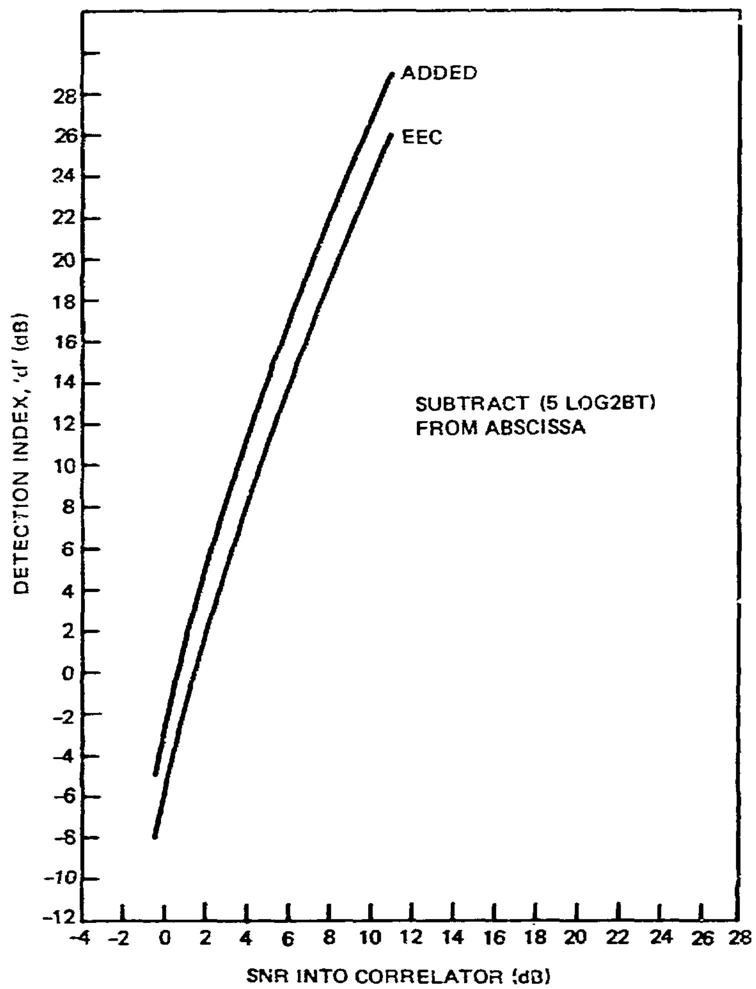

Figure 8. Detector output correlator input SNR transfer, EEC.

The preceding example shows RC to require 7.5 dB to 8.5 dB less S_i to attain the given K, which implies that RC is superior to EEC as a detection tool. However, this example required two assumptions. First, the echo was not distorted by the external filter so that, for RC, the processing gain of Eq. (15) holds. Experimental results have shown, however, a loss of up to 15 dB from the anticipated S_0 – a loss that would not occur with EEC. Second, the false alarm rate assigned for RC may be arbitrarily reduced for EEC simply by not computing values of $\rho_k(\lambda)$ or $\alpha_k(\lambda)$, as appropriate, for $|\lambda| > \delta$. Figure 9 shows a plot of K vs. d_i for different values of γ [Eq. (25)]. To complete the previous example, if $\gamma = 0.01$, then for $K = 10^{-2}$, the EEC technique requires that $d_2 = 10.5$ dB. From Fig. 8, the required S_i is now −11.5 dB, or an equivalent gain in detection capability of 3 dB.

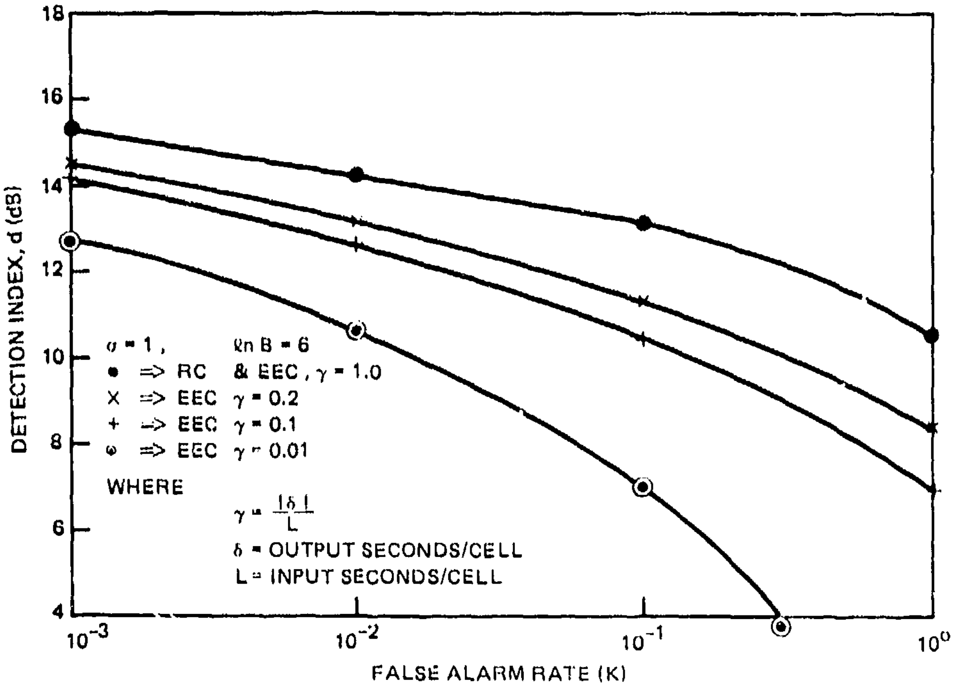

Figure 9. False alarm rate vs. detection index.

EXPERIMENTS AT SEA

EXPERIMENTAL CONDITIONS

Tests were conducted during June of 1977 at a site located approximately at 46.5°N latitude, 12.8°W latitude. The water depth was approximately 4150 metres, and the sea state was a moderate three. The transmit/receive platform was HMS MATAPAN, a converted WW II battle destroyer with a side-mounted planar array sonar. The submarine target was at a depth of 100 m. The majority of the trials occurred during parallel course (zero relative velocity) operations with a target aspect angle of approximately 100 deg. The sonar beam depression/elevation angle (D/E) ranged from 45 to 26 deg relative to the mean sea surface. The acoustic path was a single bottom bounce, and the limiting interference about the echo was reverberation from the sea surface above the target (see Fig. 10). All

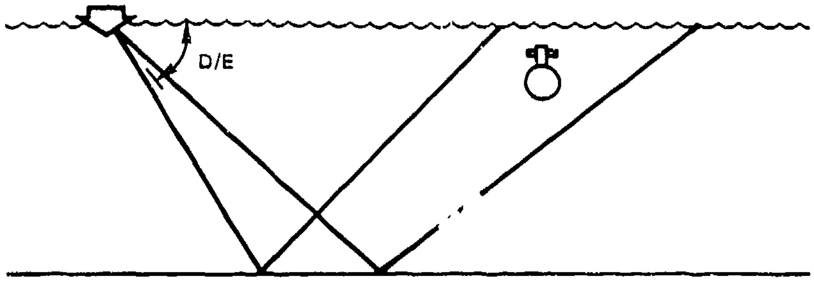

Figure 10. Experimental geometry.

transmissions were corrected for the motions of the platform, but the received signal was not so corrected prior to recording on magnetic tape.

SIGNAL PROCESSING

The narrowband signals were sampled at 1024 samples/sec – approximately 2.5 times the Nyquist folding frequency. For RC, a replica of the transmitted pulse was also sampled. The correlations (Eq. (20)) were computed via a Fast Correlation technique (Ref. 7), and the results plotted. For EEC, the output segments are for $|\lambda| \leq \delta = 10^{-3}$ seconds of correlation. The input segment duration was the pulse repetition period, L = 0.5 sec or 0.6 sec, depending on the test, giving $\gamma = 2 \times 10^{-3}$, or 1.67×10^{-3}, respectively.

EXPERIMENTAL RESULTS

Although the object of this experiment was to compare echo detectability using RC and EEC, only a limited amount of data were obtained, and the errors and uncertainties in the data made quantitative measurements impossible. However, a qualitative comparison is possible from the plots that follow. These plots are presented in groups, with the first plot in each group being a representative received time function*, z(t) [Eq. (1)], for that group of transmissions. Following this RTH are the individual RC and EEC plots for each transmission ("ping") in the group. The groups are characterized by D/E angle and pulse type, as indicated in Table 1. Each RTH has a heavy horizontal line marked "Echo Time." Because the target was equipped with a delayed acoustic transponder, it is possible to determine rather precisely the expected echo time from the target. Each correlation plot has a similar line marked "Period of interest," indicating the anticipated echo correlation time.

Figure 11b shows EEC output as anticipated from theory. There is a single strong peak with two smaller side peaks equally spaced on either side of it. These three peaks occur precisely at $\lambda = 0$ for their respective segments. Note that the corresponding RC plot, Fig. 11a, does not show an acceptably high enough echo correlation to reasonably declare an echo to be present. Most of the remaining plots in this group show more than the anticipated two or three peaks for EEC, which, it is assumed, is accounted for by some unknown acoustic paths. The nature of these paths is beyond the scope of this report. It is apparent,

*The received time function here is referred to as a Reverberation Time History (RTH). Since the background interference for these tests is dominated by acoustic returns from environmental scatterers, hence "reverberation."

Table 1. Experimental parameters.

Figure	D/E	BW	PT	Ping Numbers
11	26	400	LPM	438-442
12	26	600	LPM	443-447
13	35	500	PRN	224-225
14	35	400	LPM	219-223
15	40	400	LPM	147-155
16	45	400	LPM	82-87

Where: D/E in degrees, BW is pulse bandwidth in Hz, and PT is pulse type.

however, that at this D/E, EEC provides a much more satisfactory target indication than does RC, which often has the echo correlations nearly buried in the background.

At steeper D/E angles (shorter ranges), the RC plots begin to improve — see Fig. 14c. However, the EEC plots are still superior in $\hat{S}_0$ — see Fig. 14d. Several of the EEC plots, such as 14f and 14h, were suppressed by the large spike at the left hand side, but the $\hat{S}_0$ is, in fact, higher than that for the corresponding RC.

At the steeper D/E angles of 35 and 45 deg, the high output from EEC in the first seven to fifteen segments indicates correlated echoes from the bottom. As an example, see Fig. 15h. These returns may serve to suppress the scale for the remainder of the plot, but the geometry of Fig. 10 shows them to occur well before any possible target echoes, so that they do not, in fact, affect the signal-to-noise ratio of the target echo.

Figure 16, which shows the results for the steepest D/E of 45 deg, not only has more correlation peaks for both RC and EEC than anticipated, but the EEC peaks are not centered at $\lambda = 0$ for their respective segments. While a definitive reason for either anomaly is not apparent, the off-center peaks were most likely caused by the vertical acceleration of the receive platform during the reception time of the target echoes. For the most shallow D/E of 26 deg, any vertical acceleration of the receive platform would have produced only a minor projection along the beam axis, and, as shown in Fig. 11, the peaks are constrained to $\lambda = 0$.

The enhancement process discussed earlier (Eq. (20)) was not used on these data because of the peaks not being constrained to segment center ($\lambda = 0$).

In order to compare empirical results with theoretical predictions, one requirement is that the background noise statistics be the same as those used in the predictions. The various RTH plots show pronounced variations in background intensity, so that the concept of noise stationarity does not hold. However, it is possible to reduce the effects of a slowly time varying background by the number of methods. One might pass the correlator/detector output through a suitable high pass filter, or, perhaps, since the correlation may be accomplished with the cross spectrum, by dividing the cross spectrum by the auto power spectra of both components in the correlation. It appears, however, that the EEC plots have

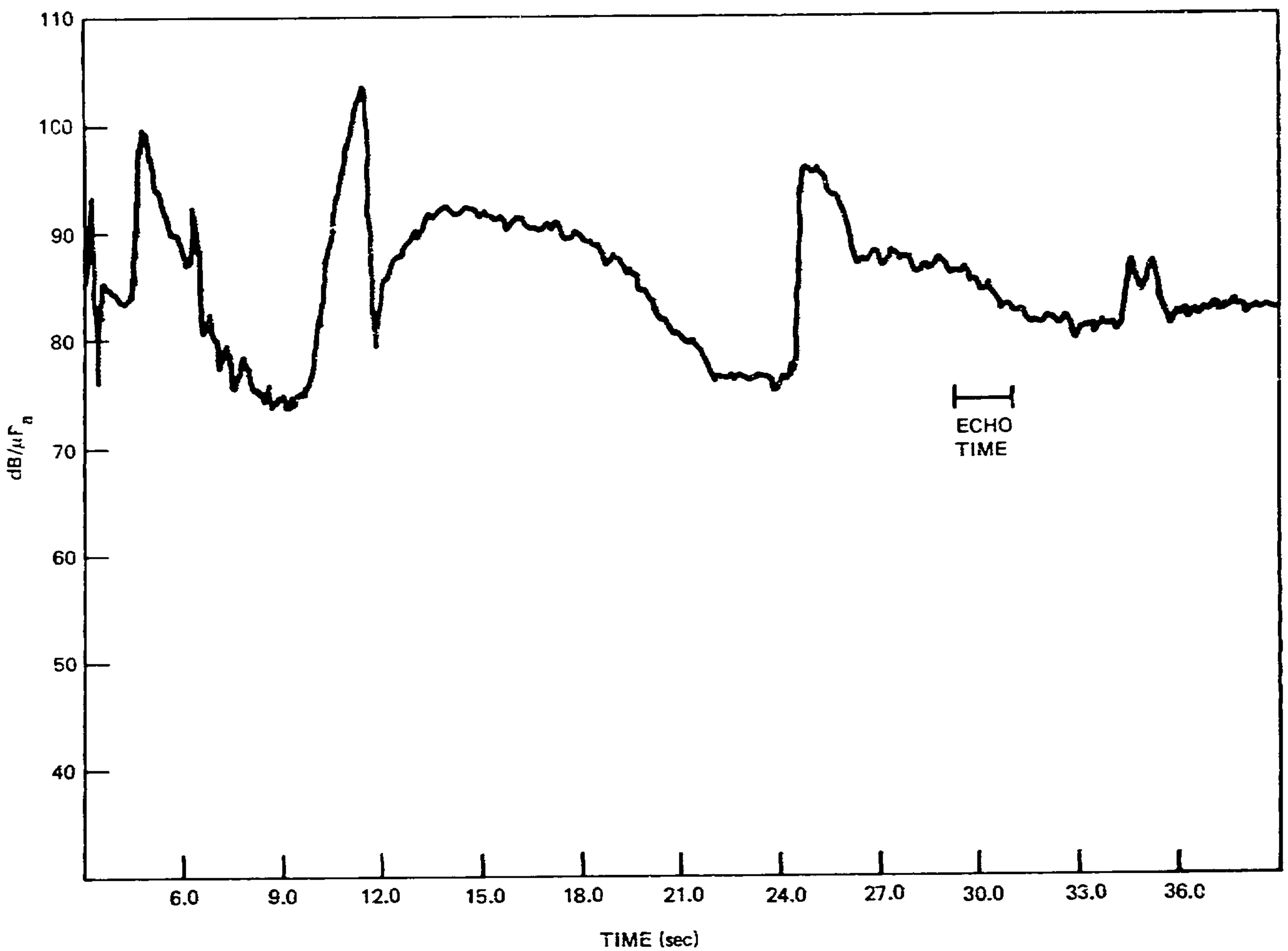

Figure 11. Reverberation time history, D/E 26°.

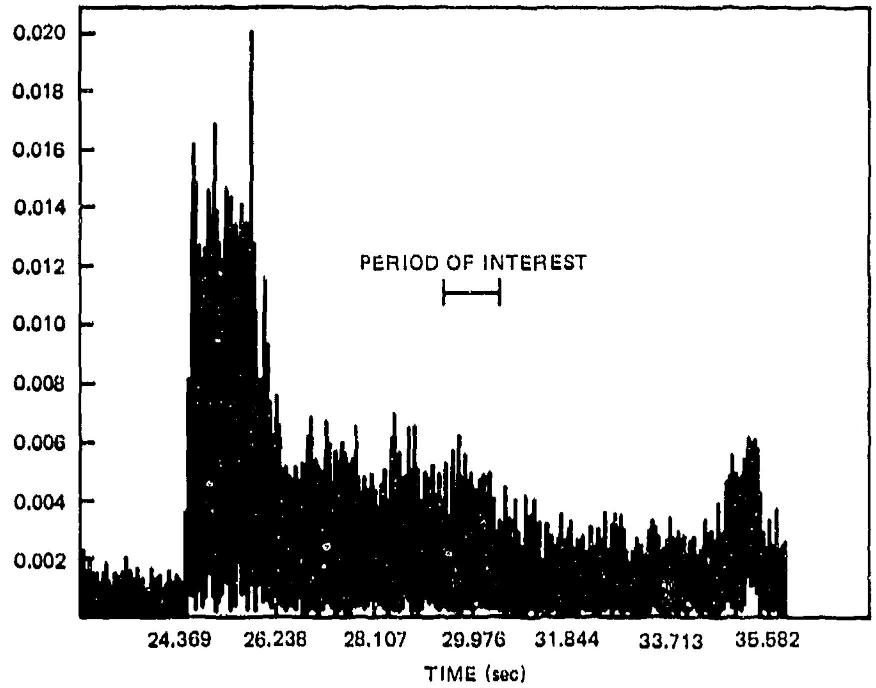

Figure 11a. RC (ping 443).

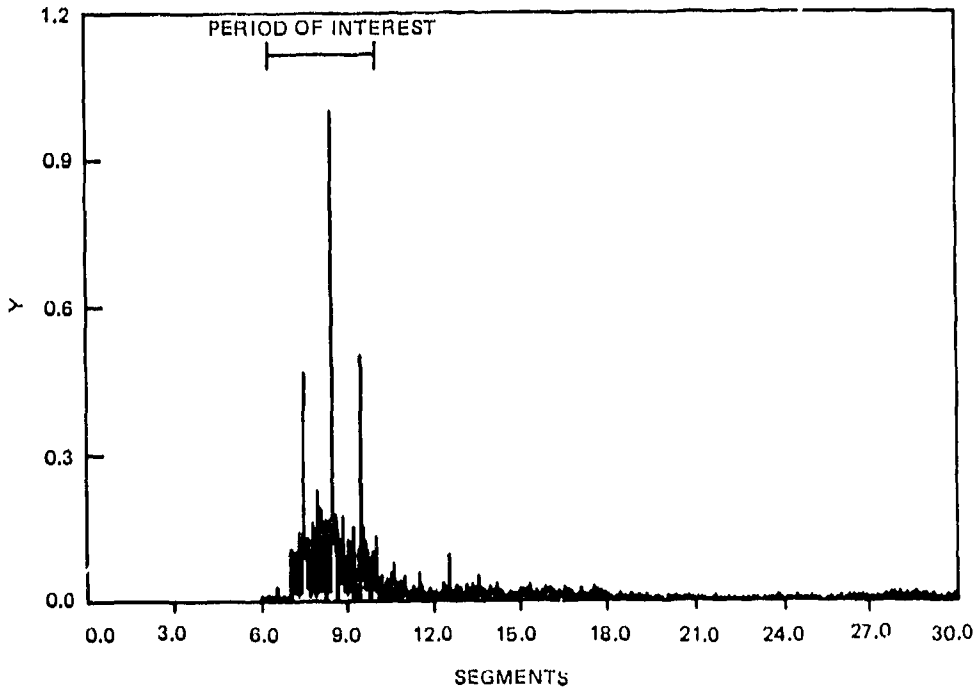

Figure 11b. EEC (ping 443).

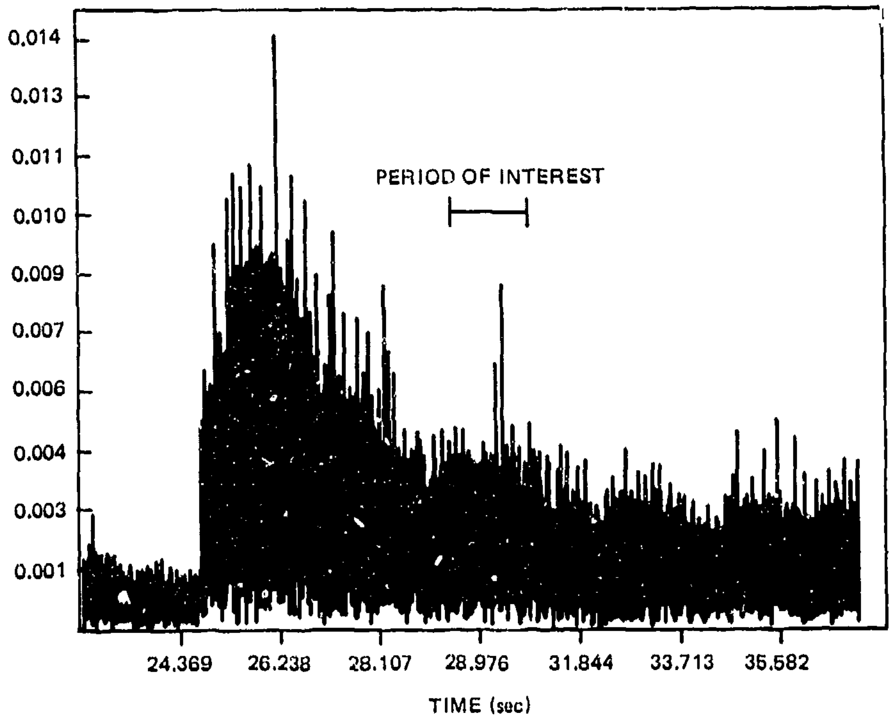

Figure 11c. RC (ping 444).

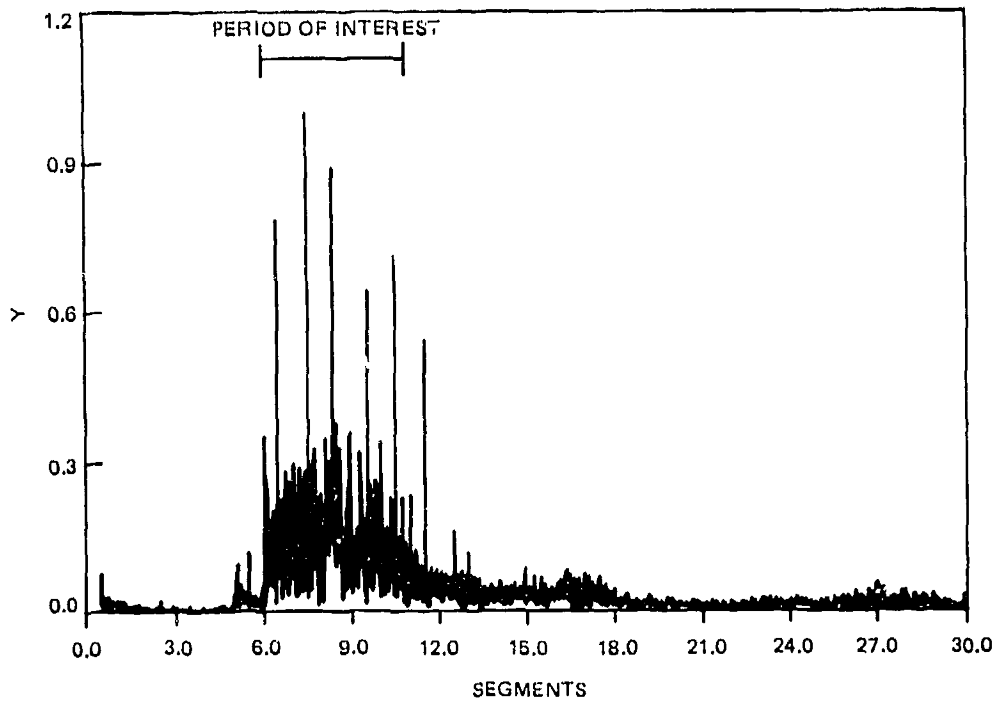

Figure 11d. EEC (ping 444).

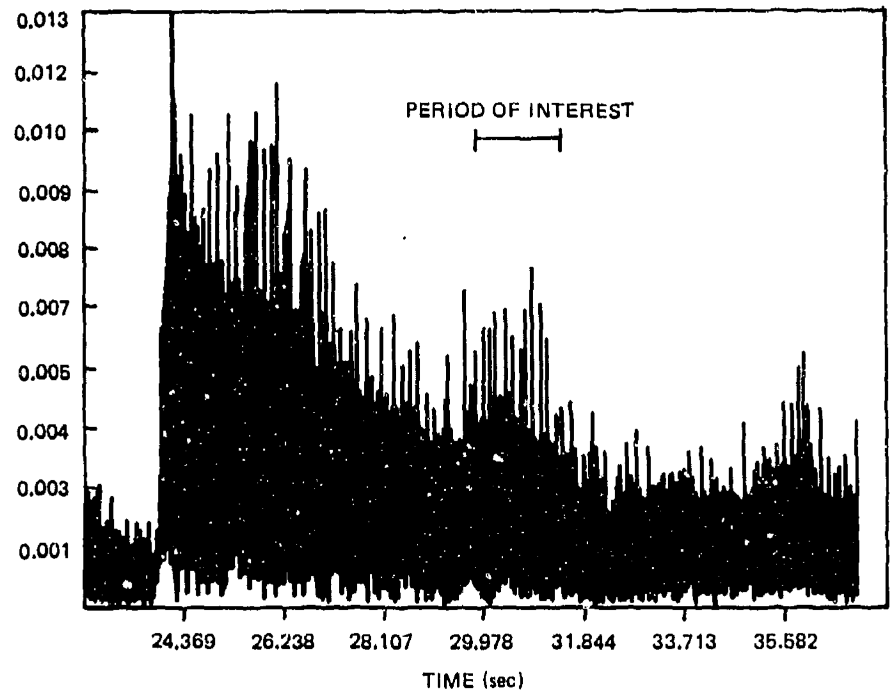

Figure 11c. RC (ping 445).

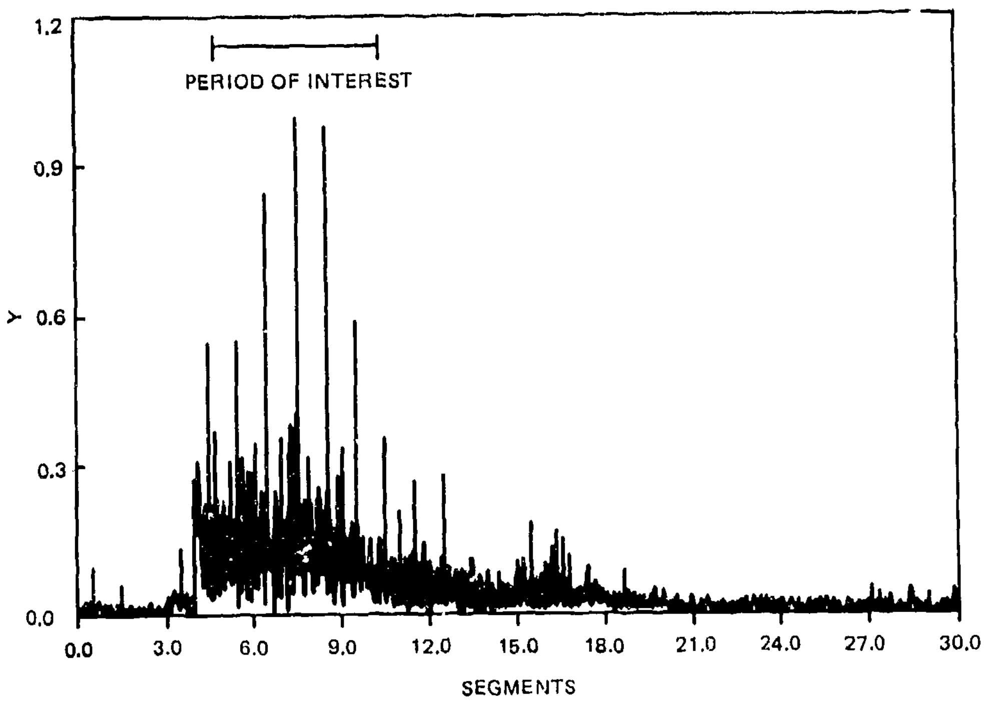

Figure 11f. EEC (ping 445).

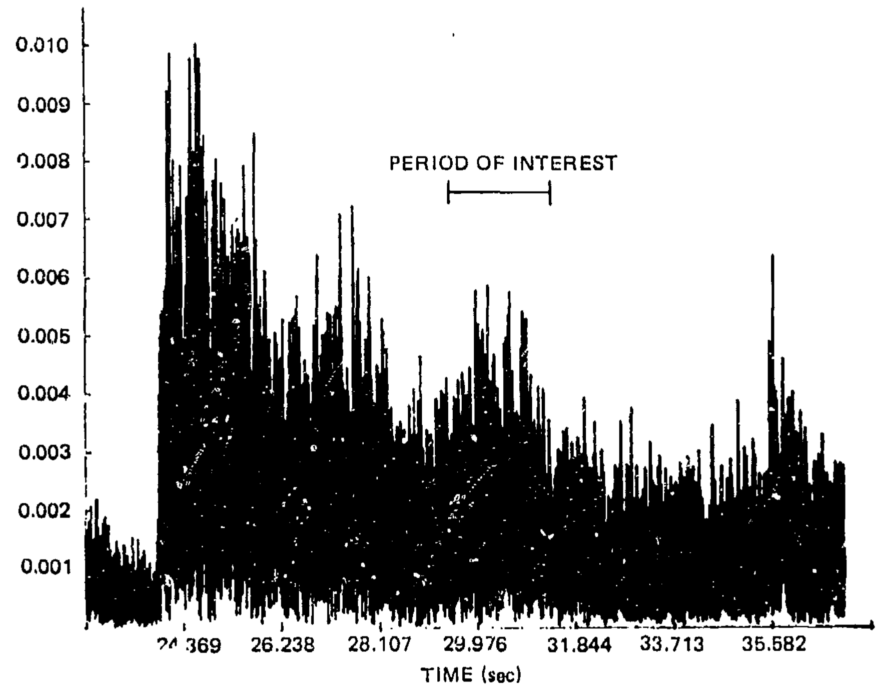

Figure 11g. RC (ping 446).

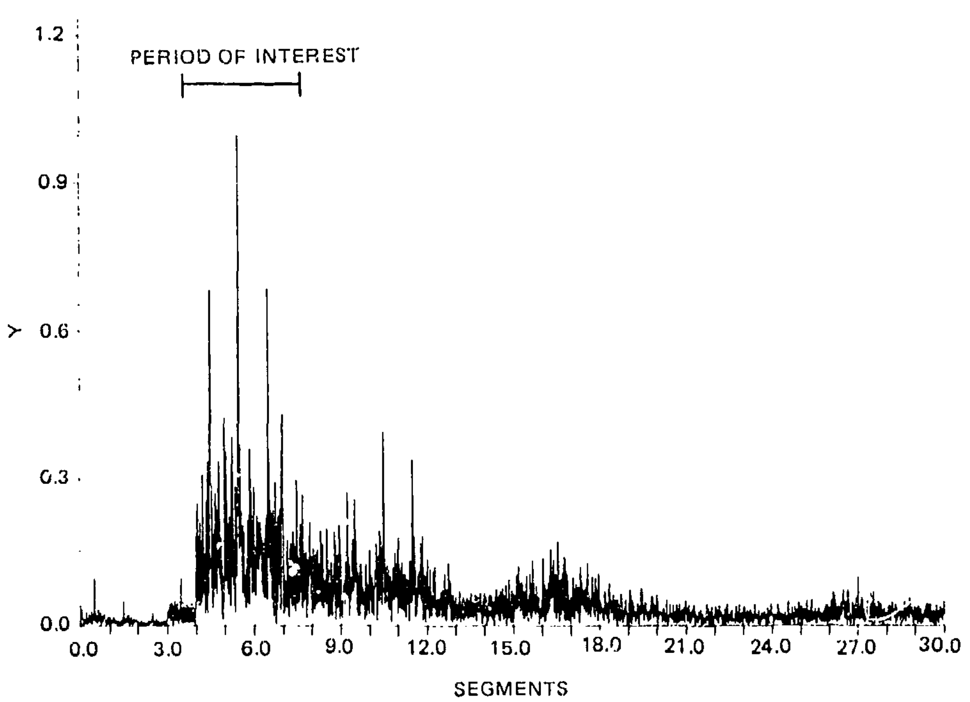

Figure 11h. EEC (ping 446).

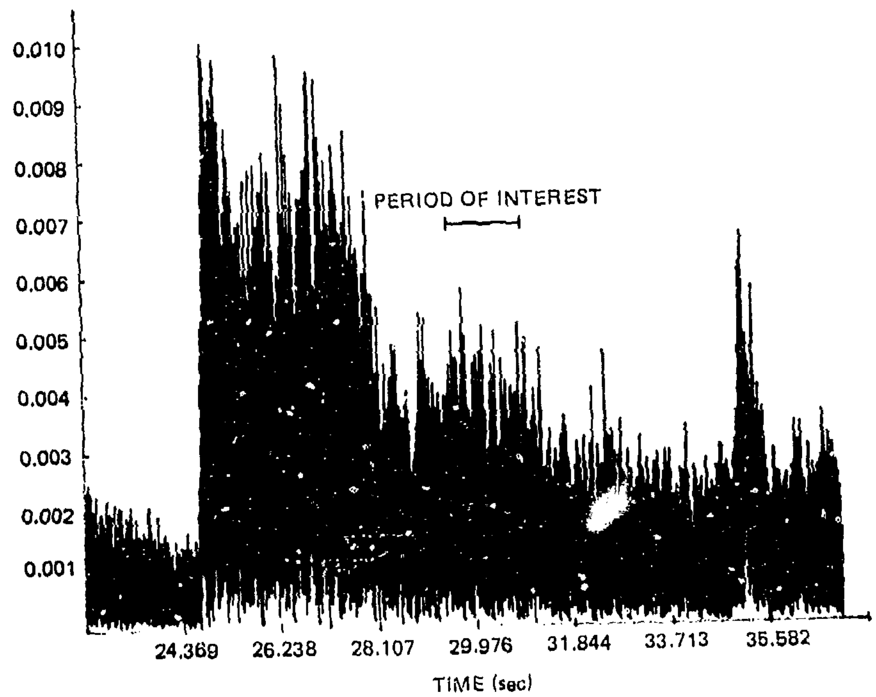

Figure 11i. RC (ping 447).

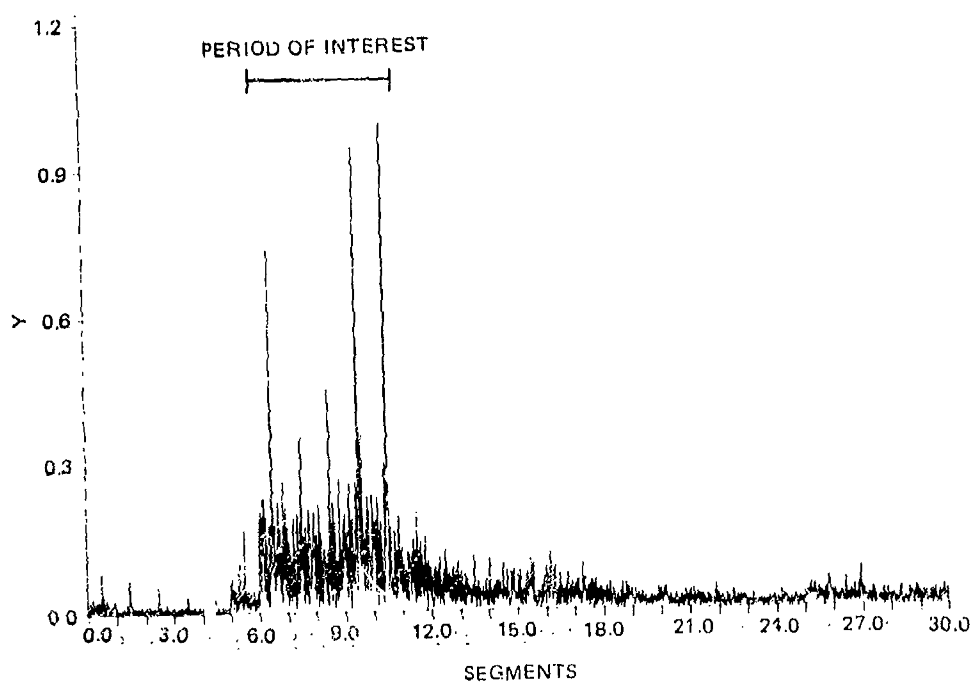

Figure 11j. EEC (ping 447).

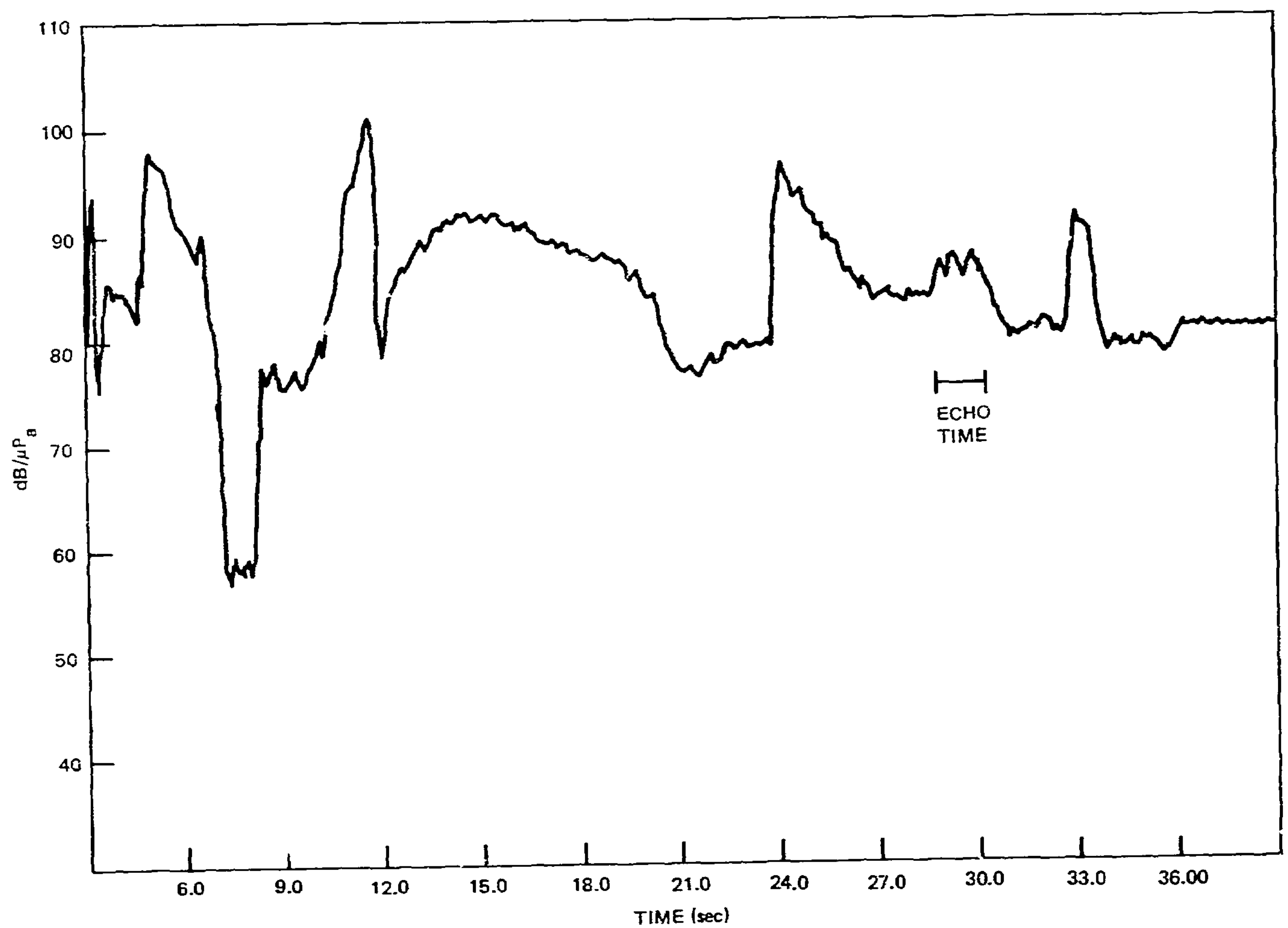

Figure 12. Reverberation time history, D/E 26°.

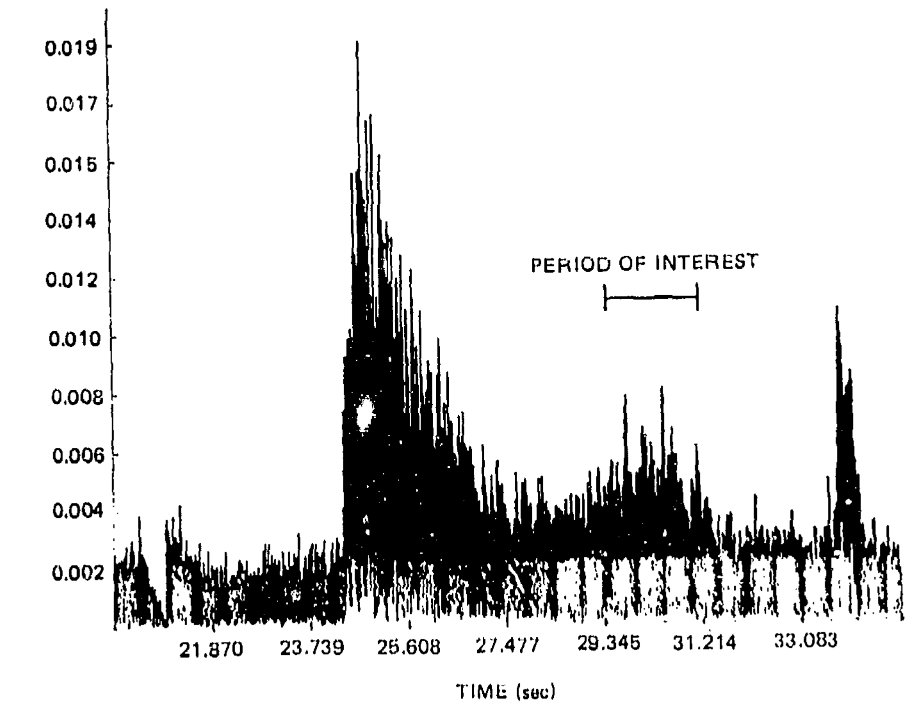

Figure 12a. RC (ping 439).

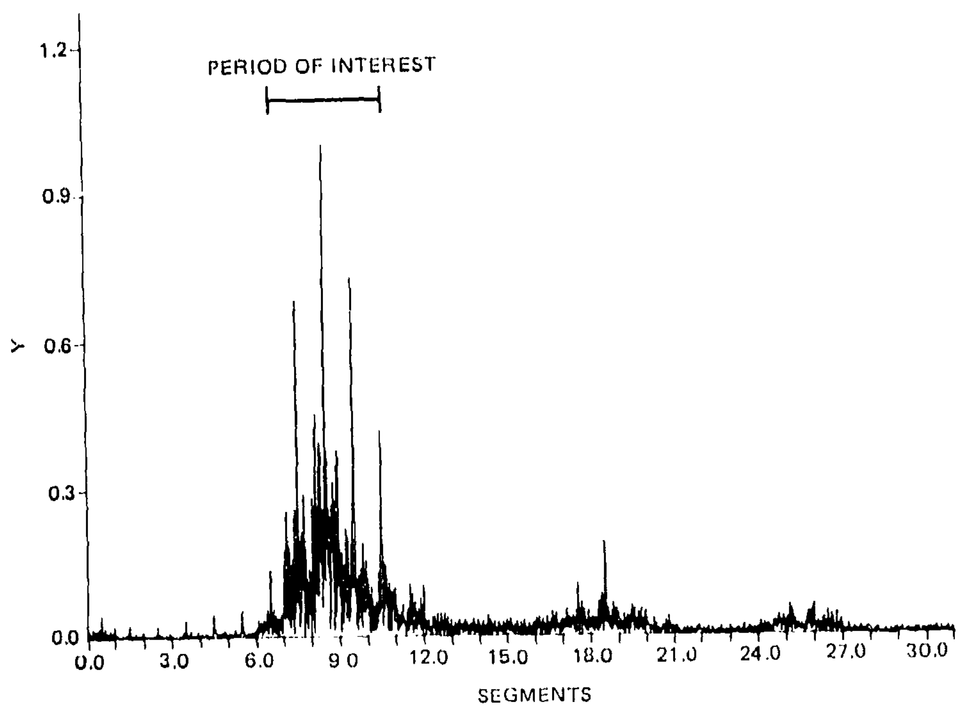

Figure 12b. EEC (ping 439).

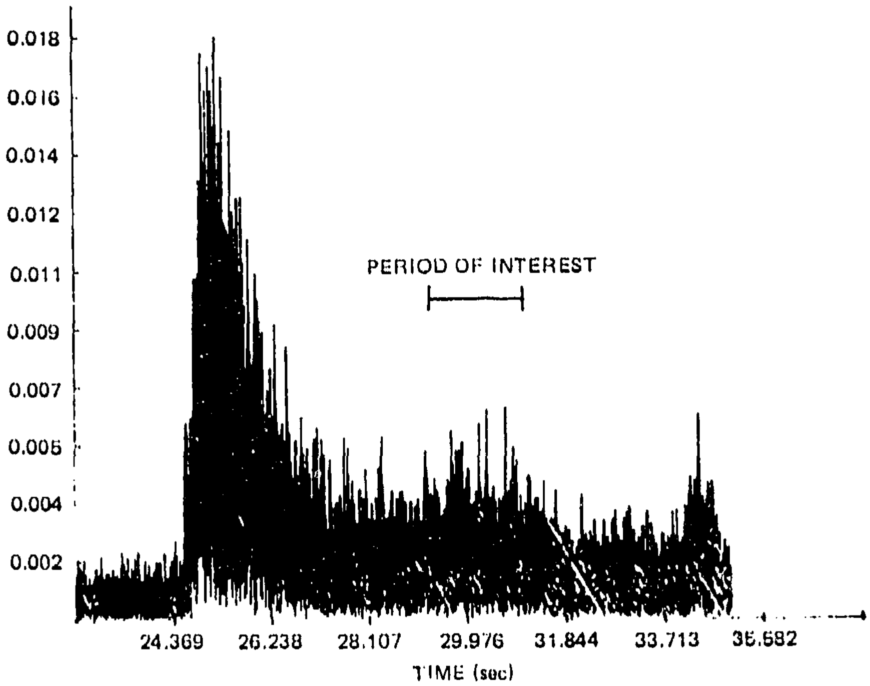

Figure 12c. RC (ping 440).

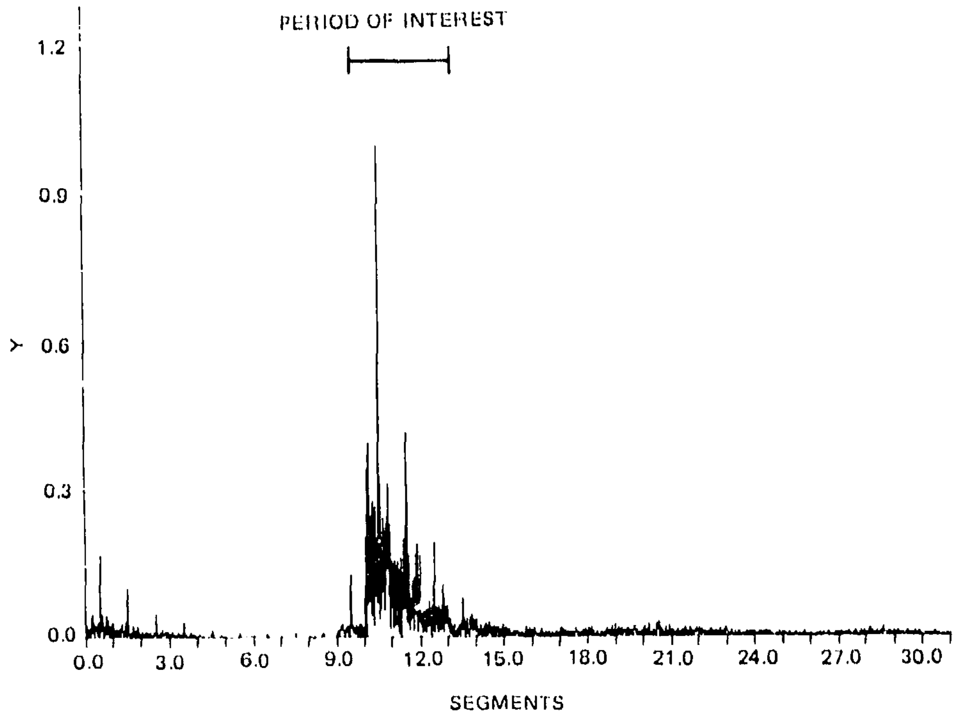

Figure 12d. EEC (ping 440).

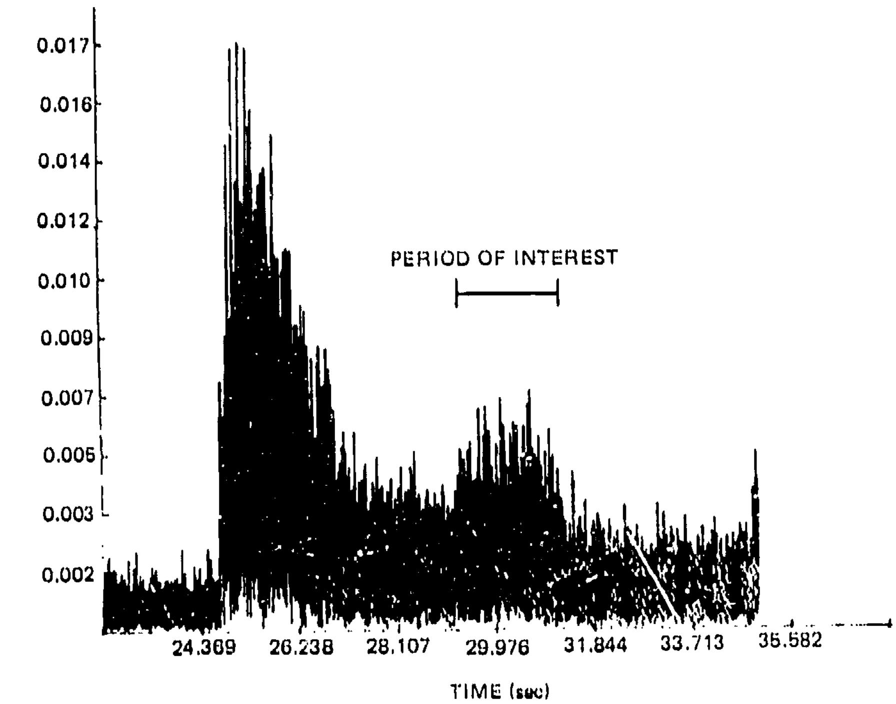

Figure 12e. RC (ping 441).

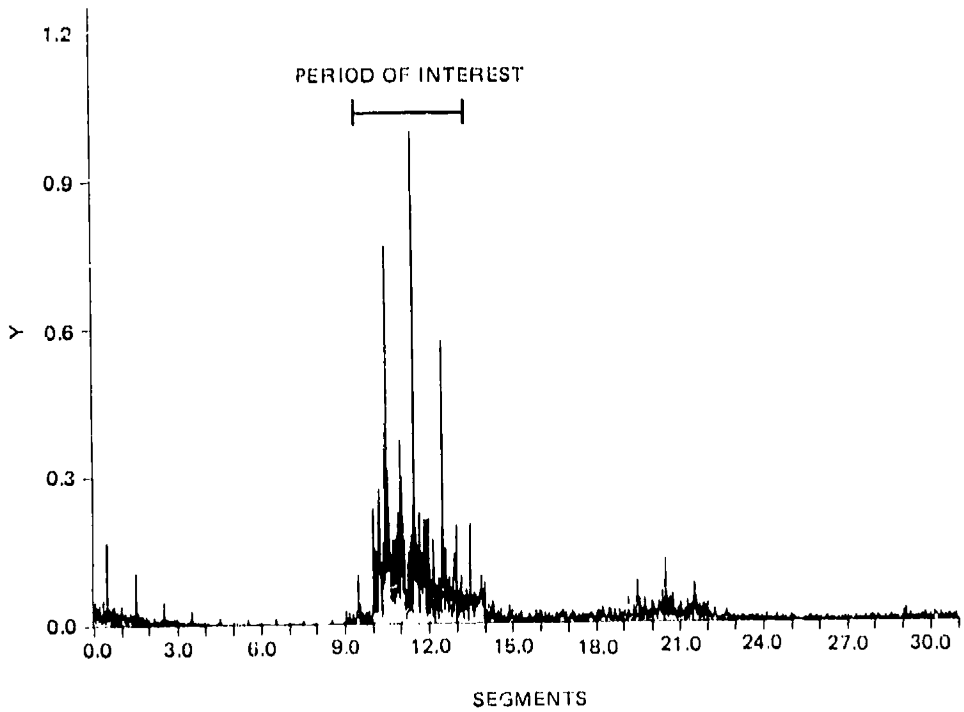

Figure 12f. EEC (ping 441).

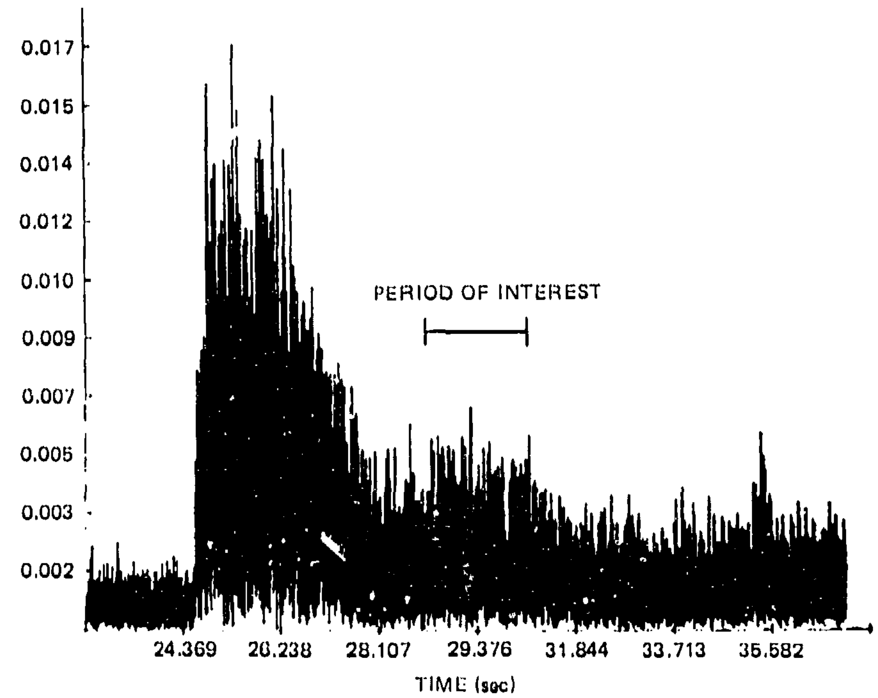

Figure 12g. RC (ping 442).

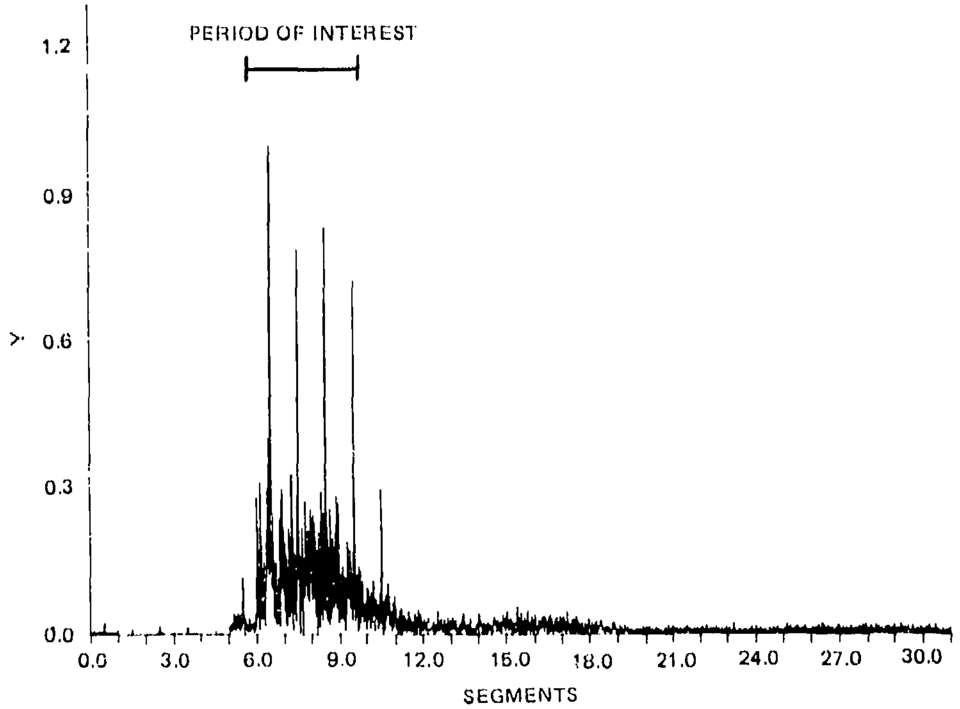

Figure 12h. EEC (ping 442).

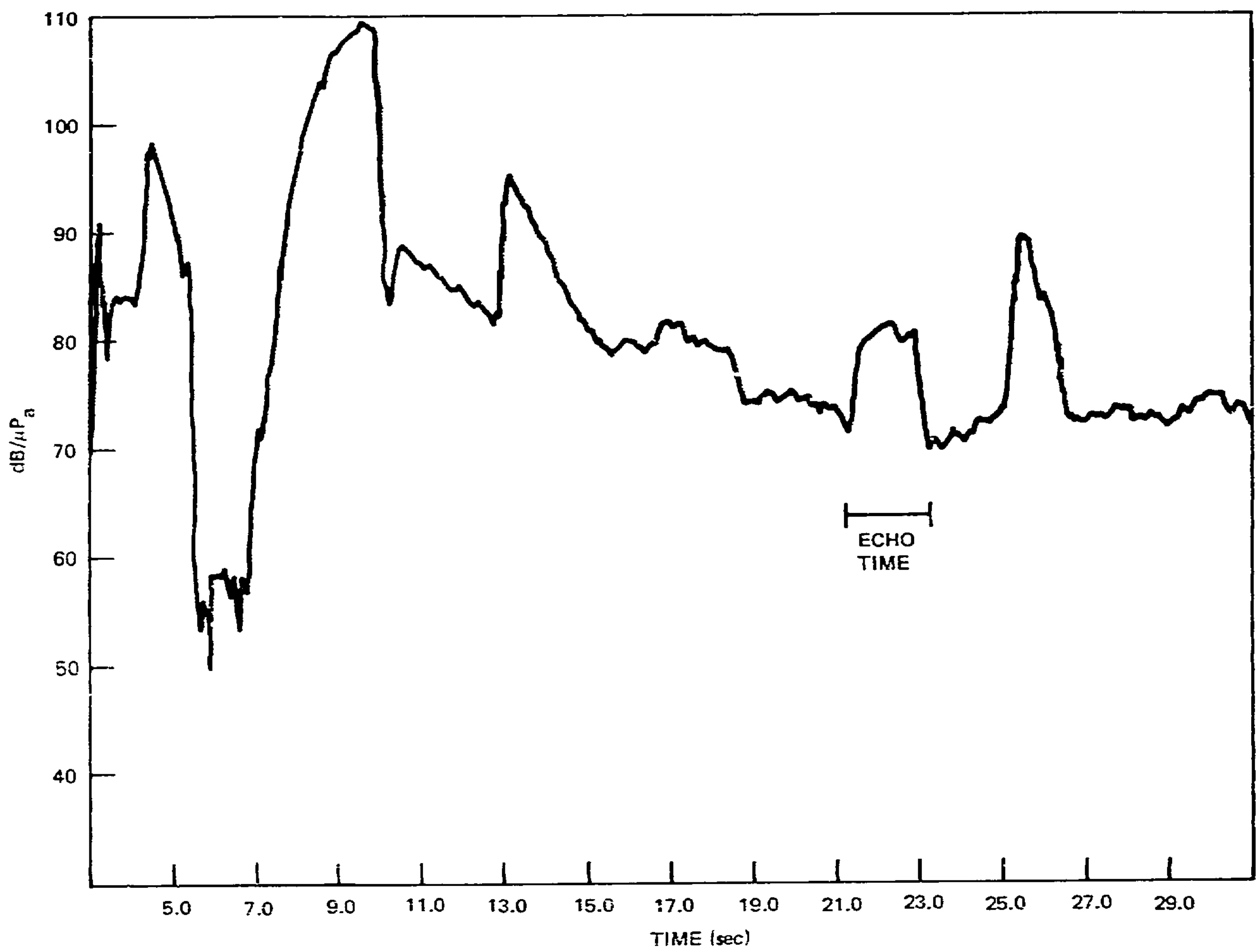

Figure 13. Reverberation time history, D/E 35°.

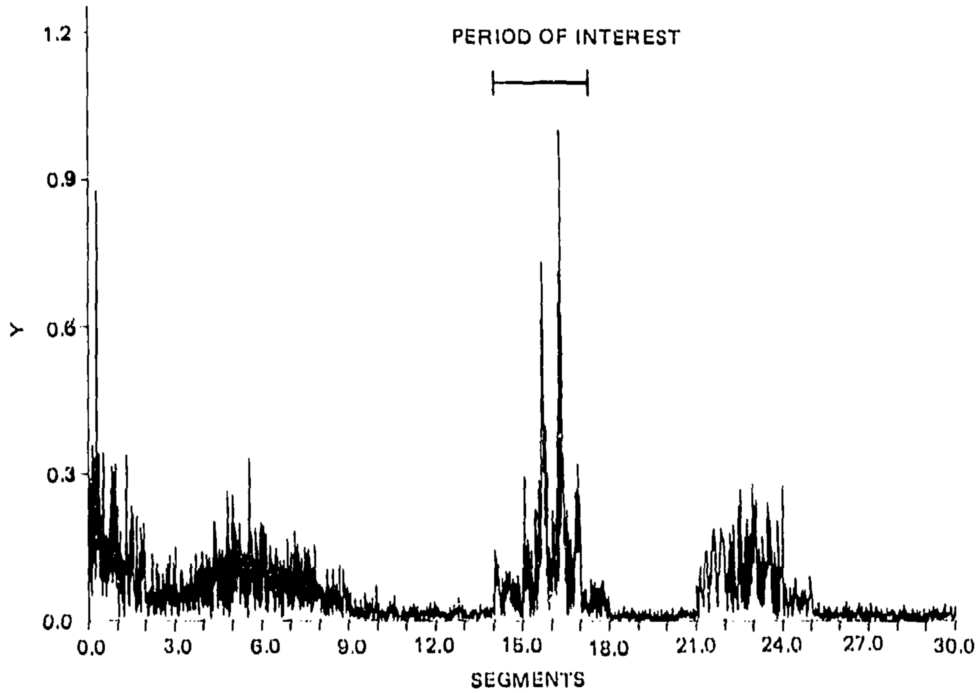

Figure 13a. EEC (ping 224).

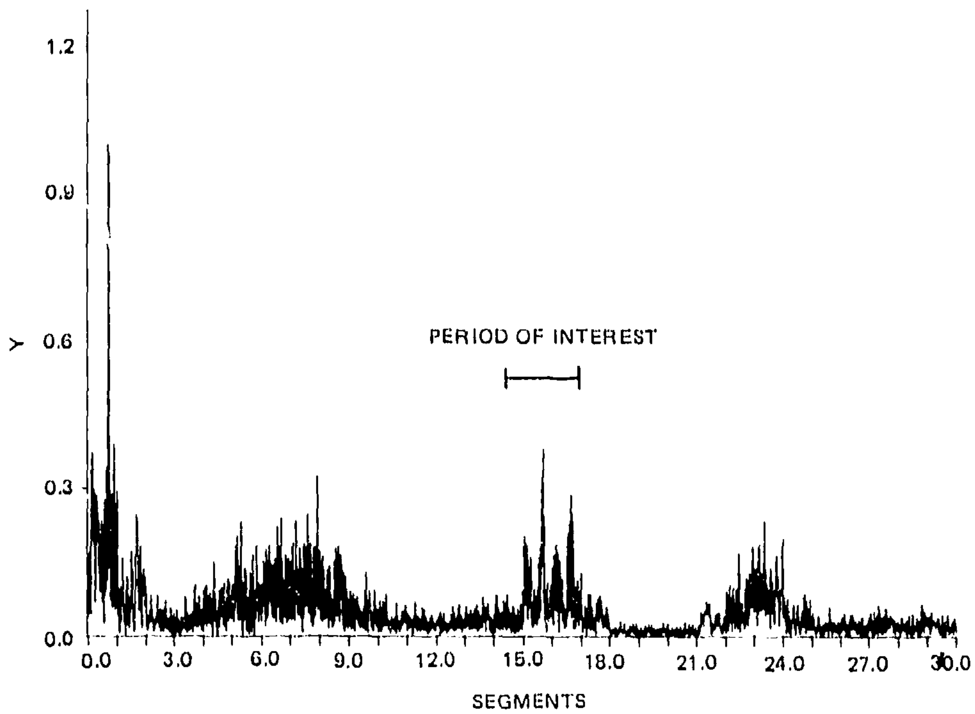

Figure 13b. EEC (ping 225).

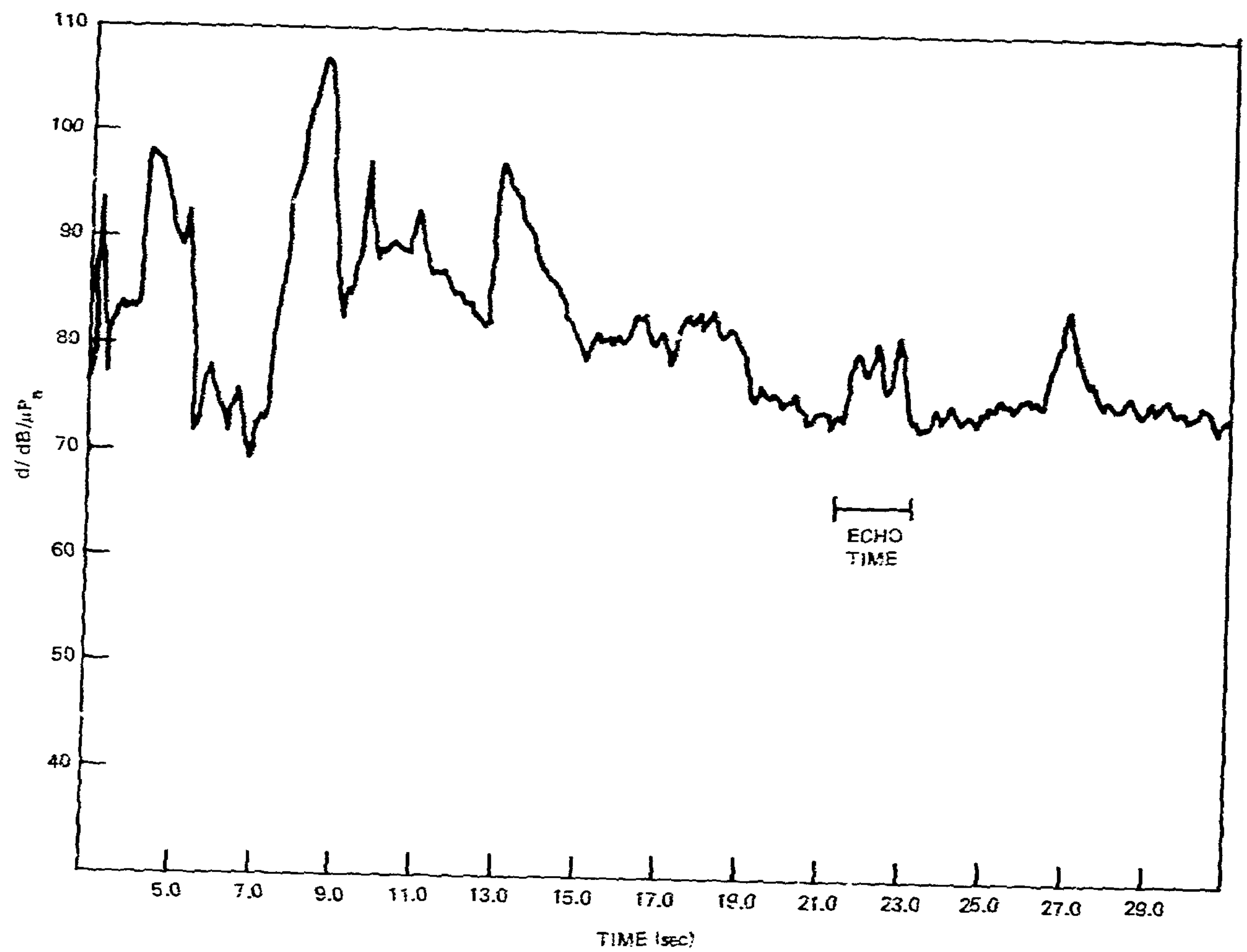

Figure 14. Reverberation time history, D/E 35°.

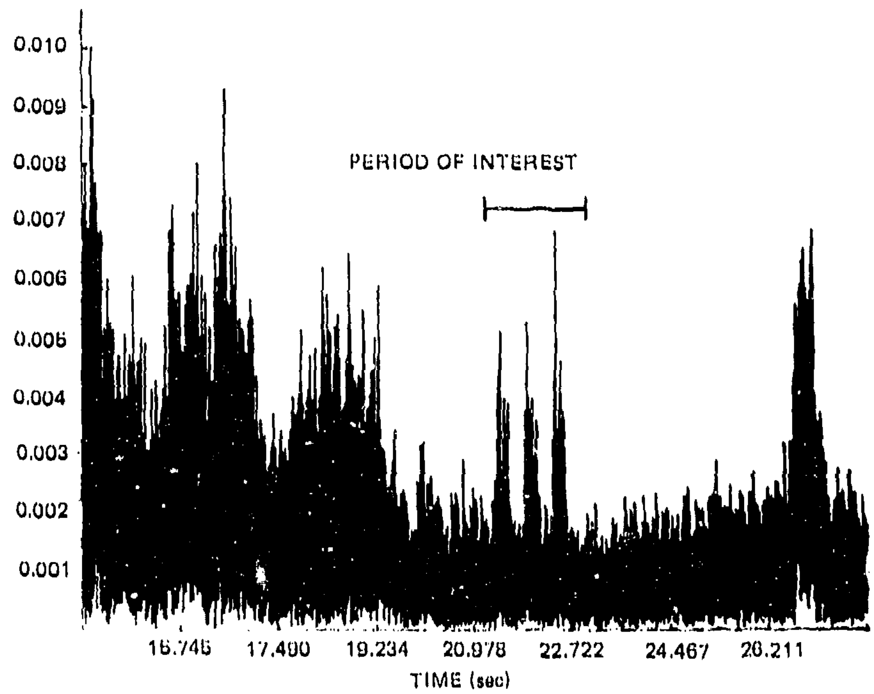

Figure 14a. RC (ping 219).

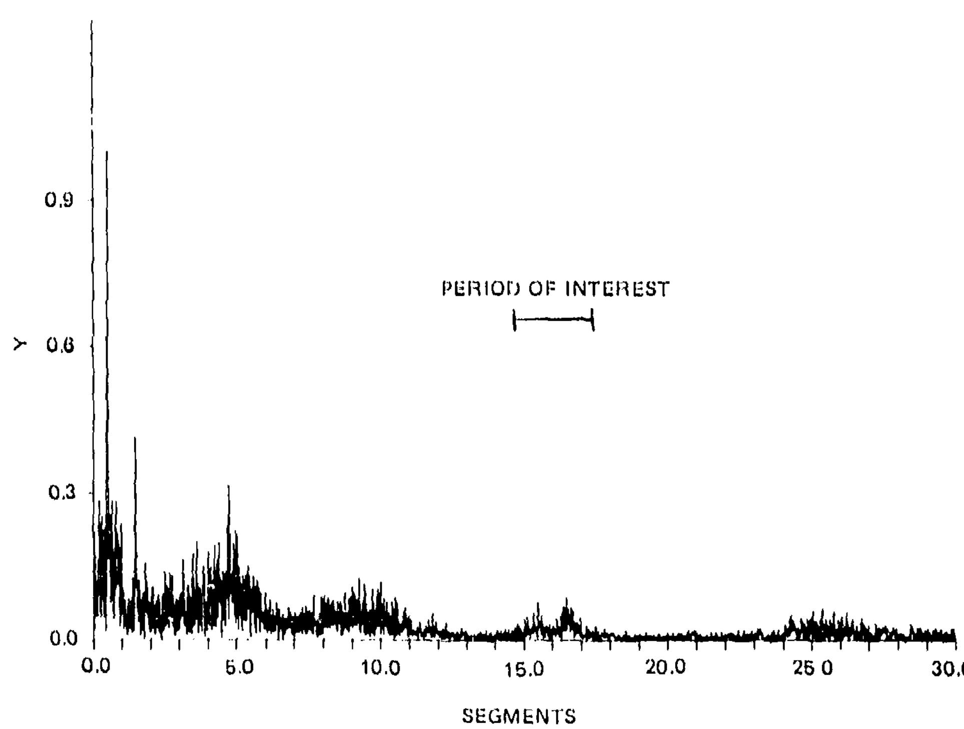

Figure 14b. EEC (ping 219).

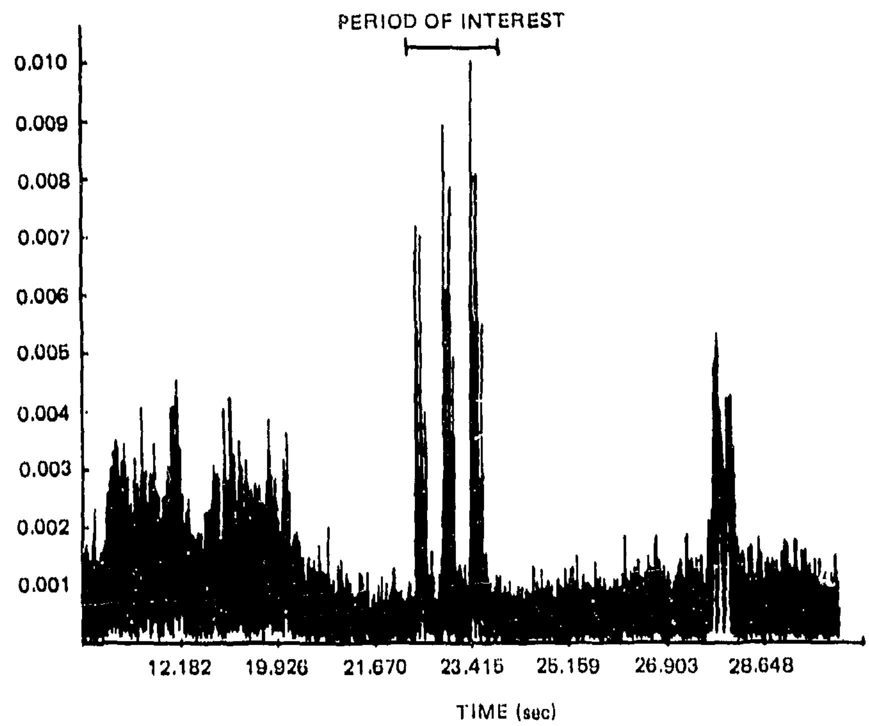

Figure 14c. RC (ping 220).

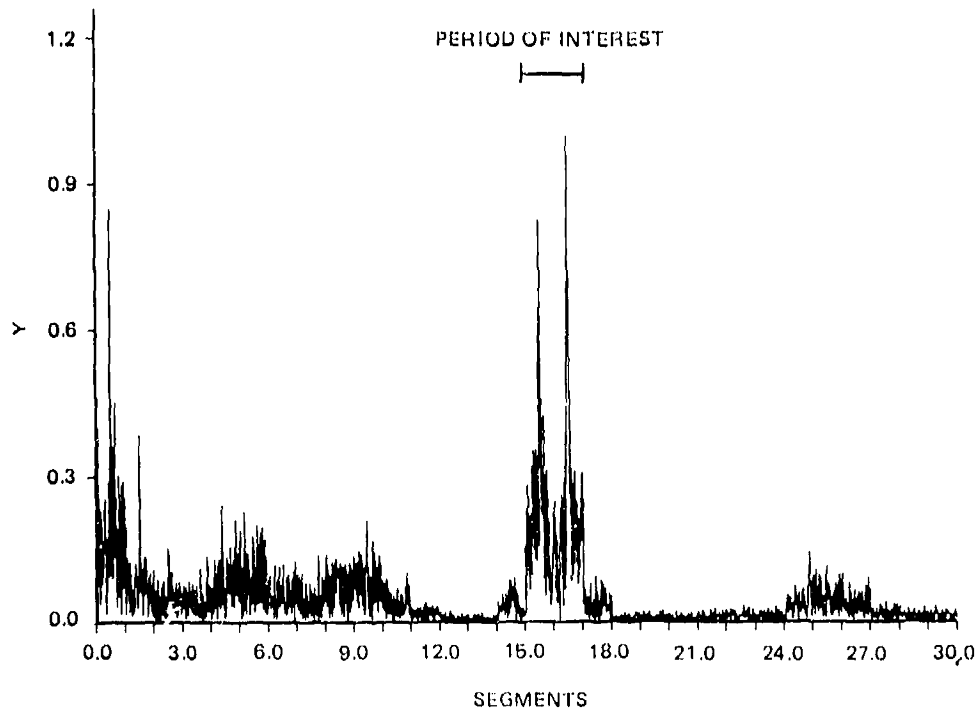

Figure 14d. EEC (ping 220).

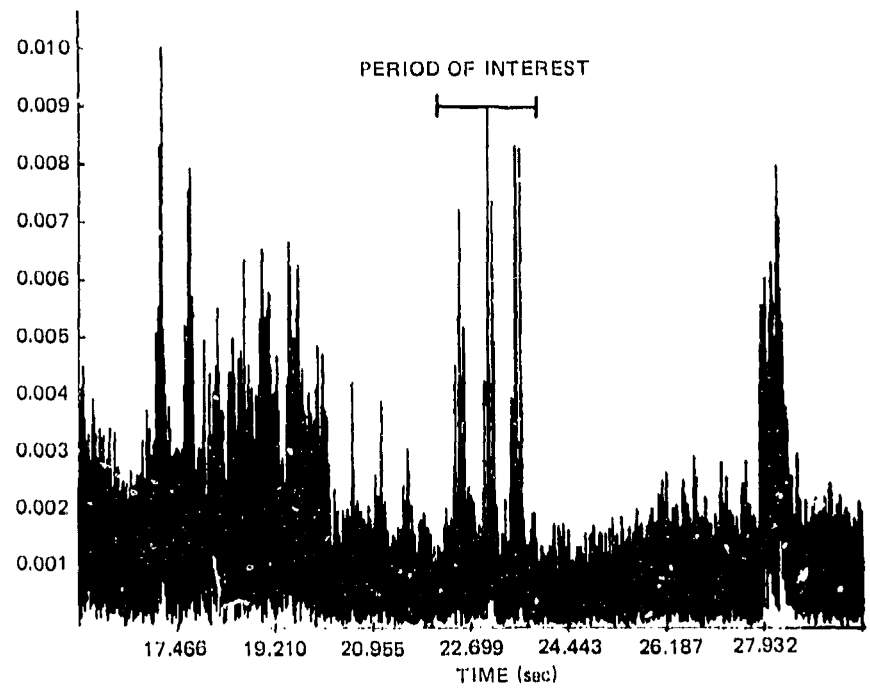

Figure 14e. RC (ping 221).

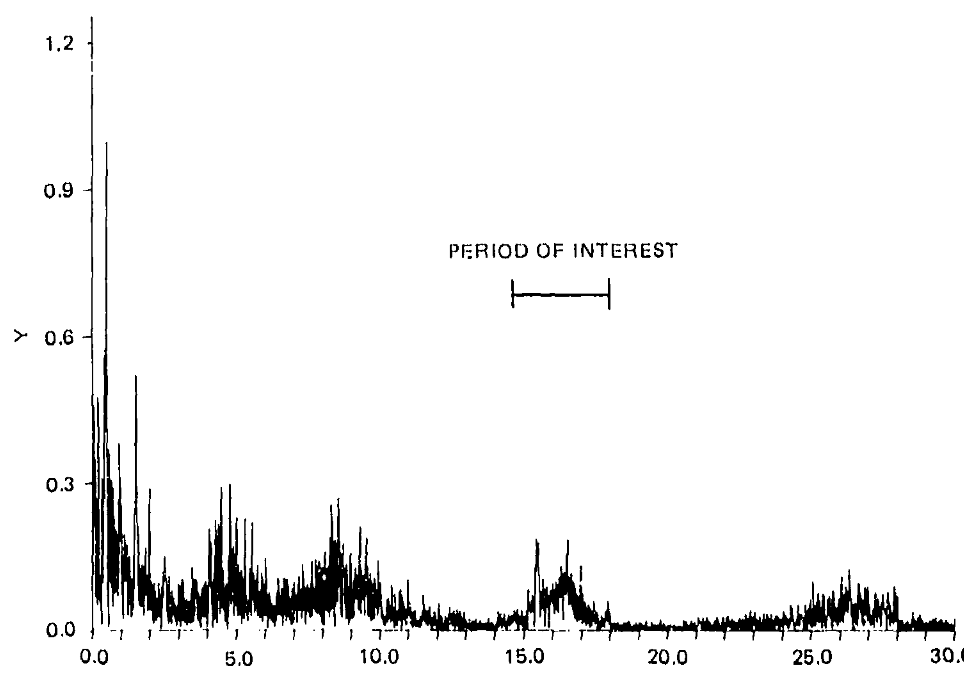

Figure 14f. EEC (ping 221).

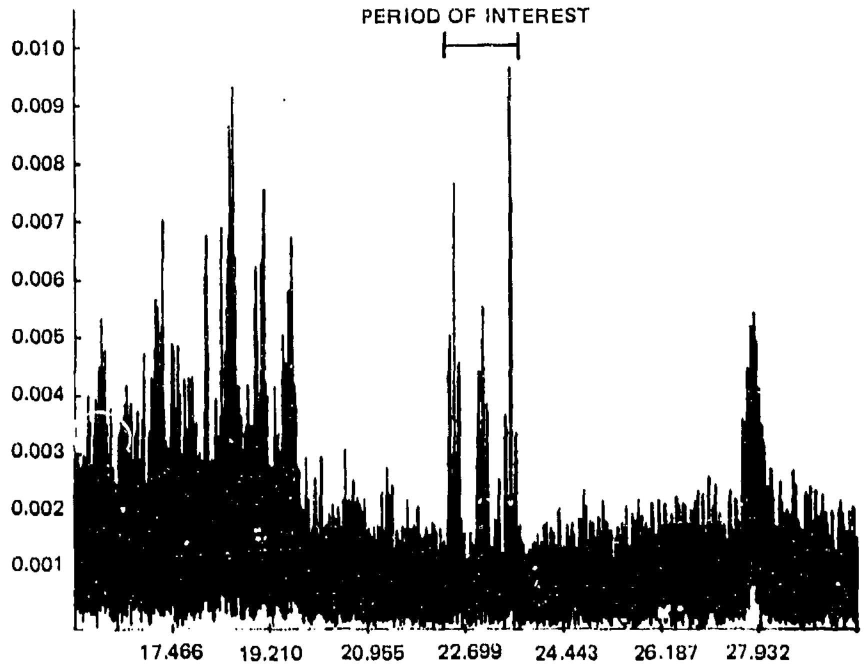

Figure 14g. RC (ping 222).

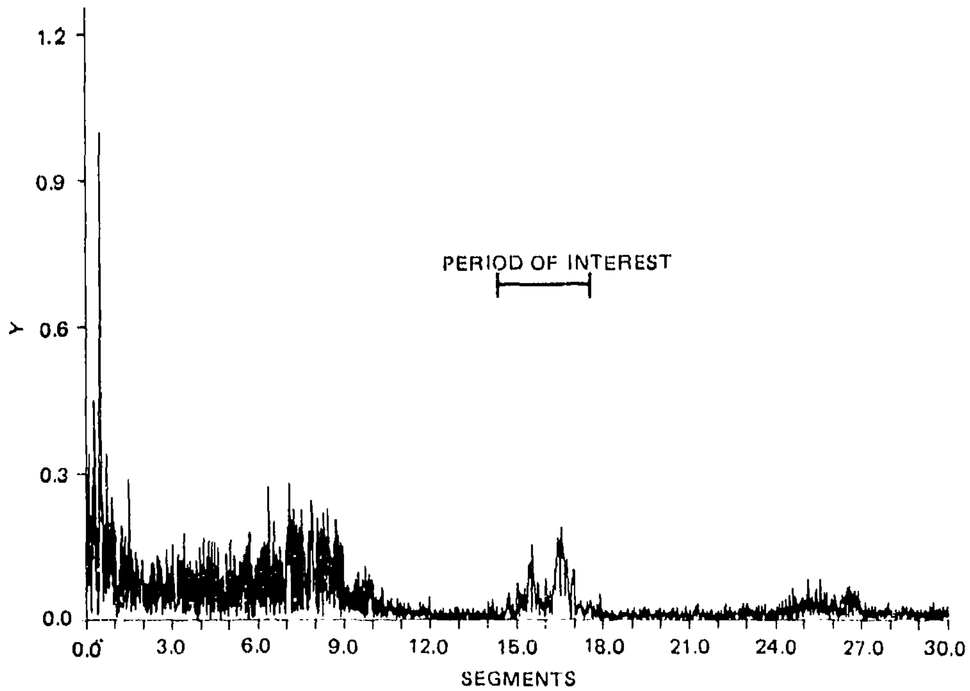

Figure 14h. EEC (ping 222).

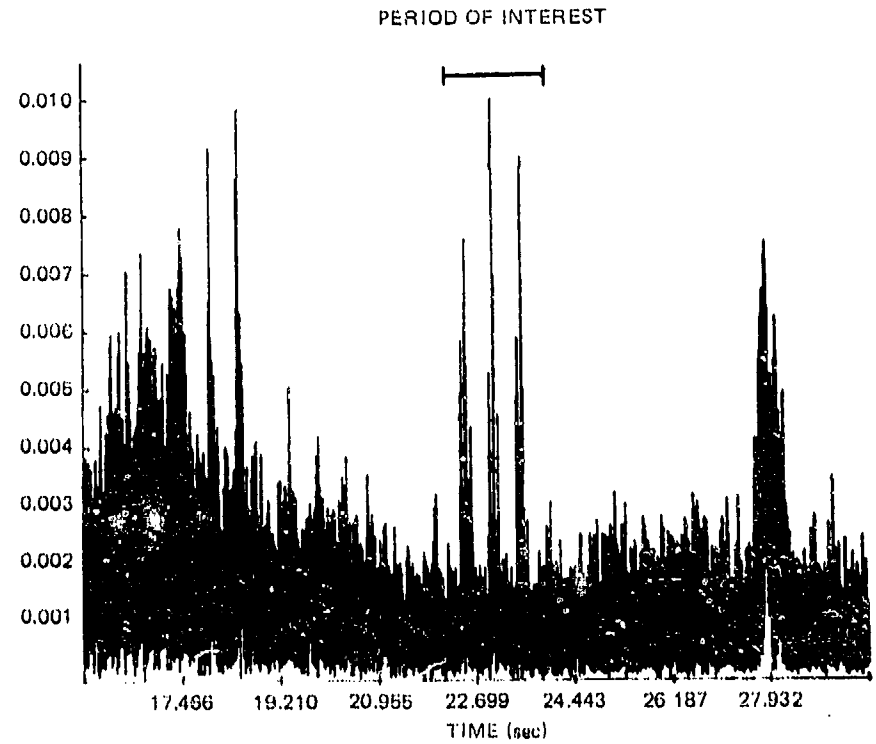

Figure 14i. RC (ping 223).

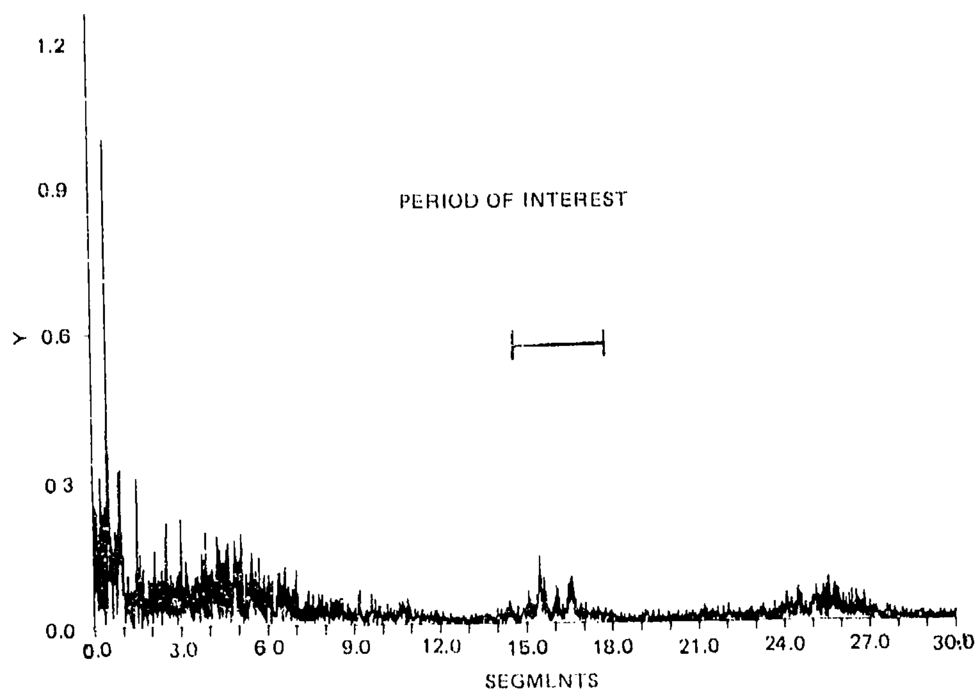

Figure 14j. EEC (ping 223).

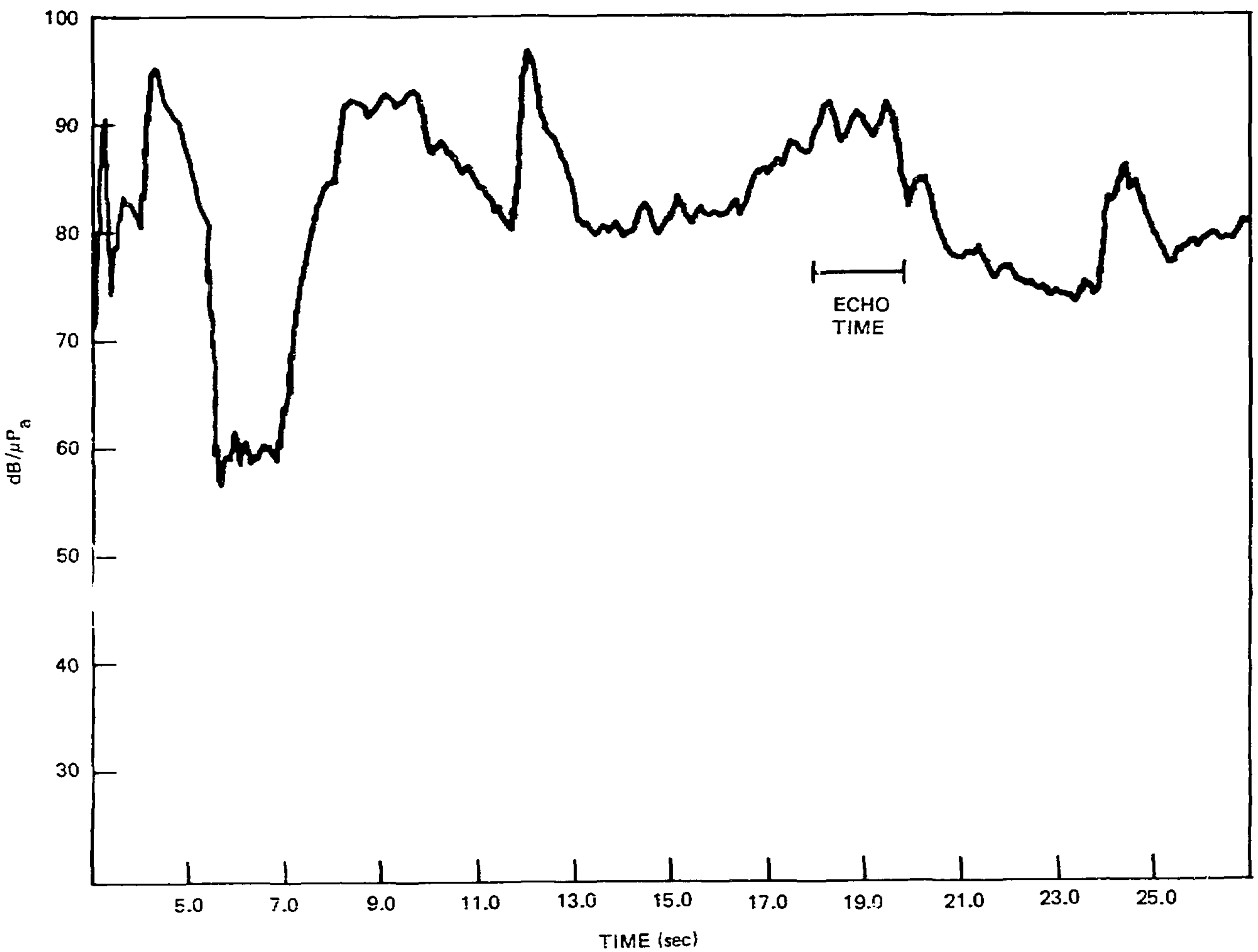

Figure 15. Reverberation time history, D/E 40°.

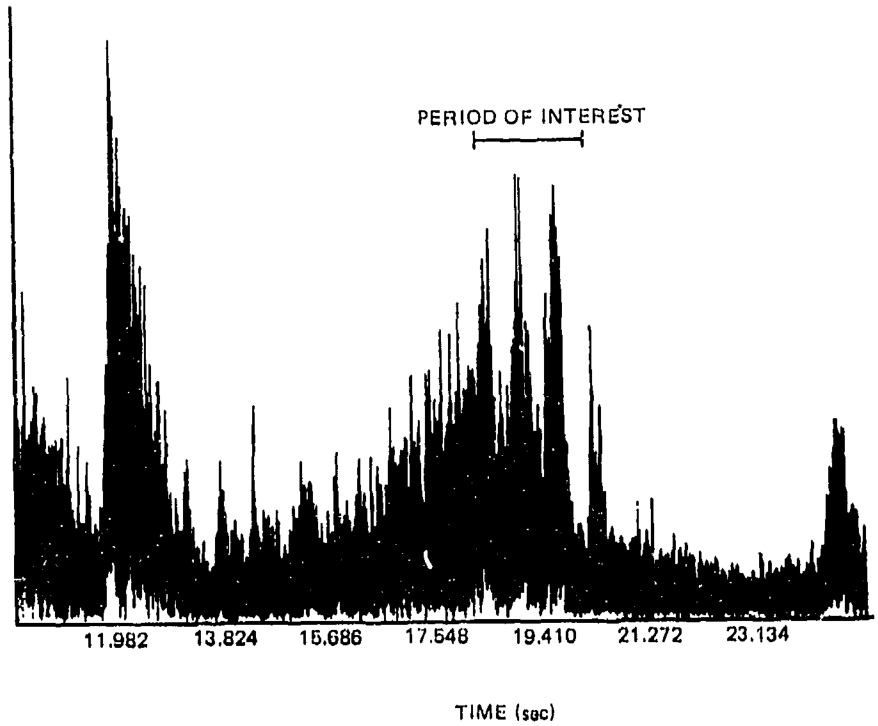

Figure 15a. RC (ping 147).

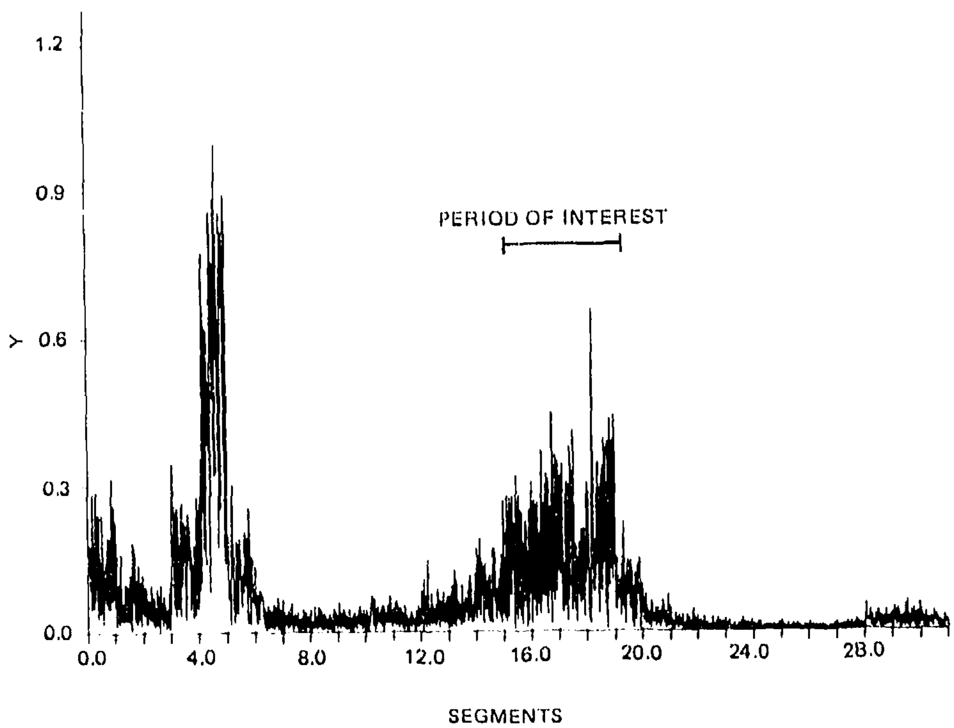

Figure 15b. EEC (ping 147).

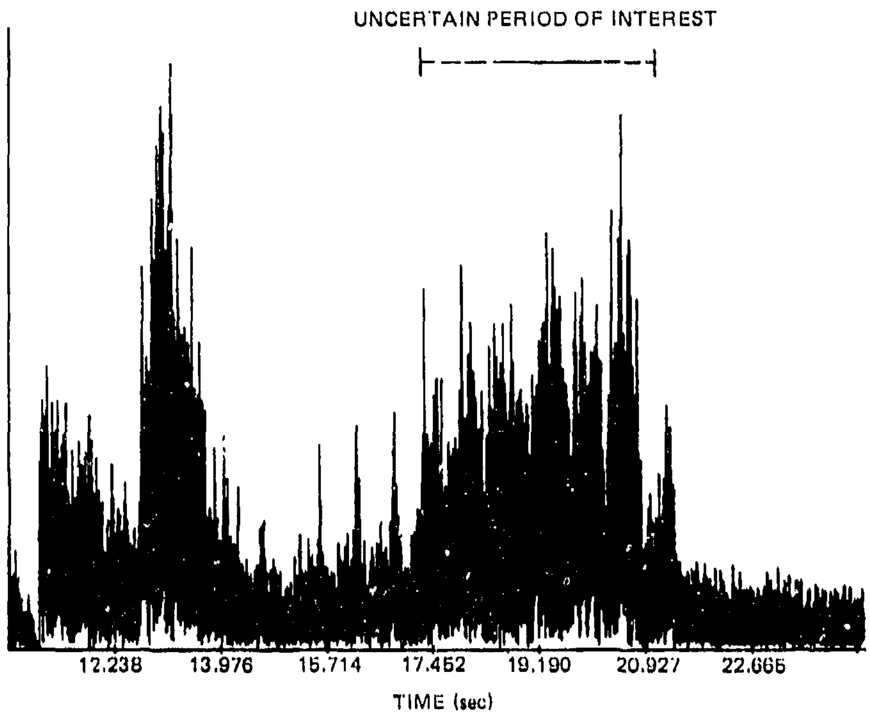

Figure 15c. RC (ping 148).

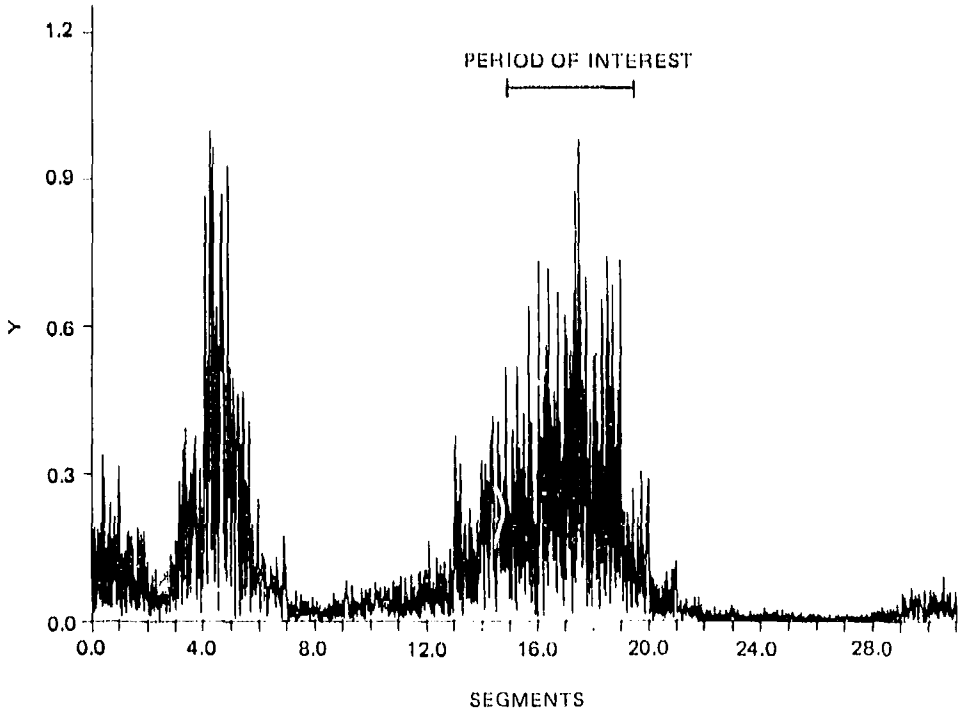

Figure 15d. EEC (ping 148).

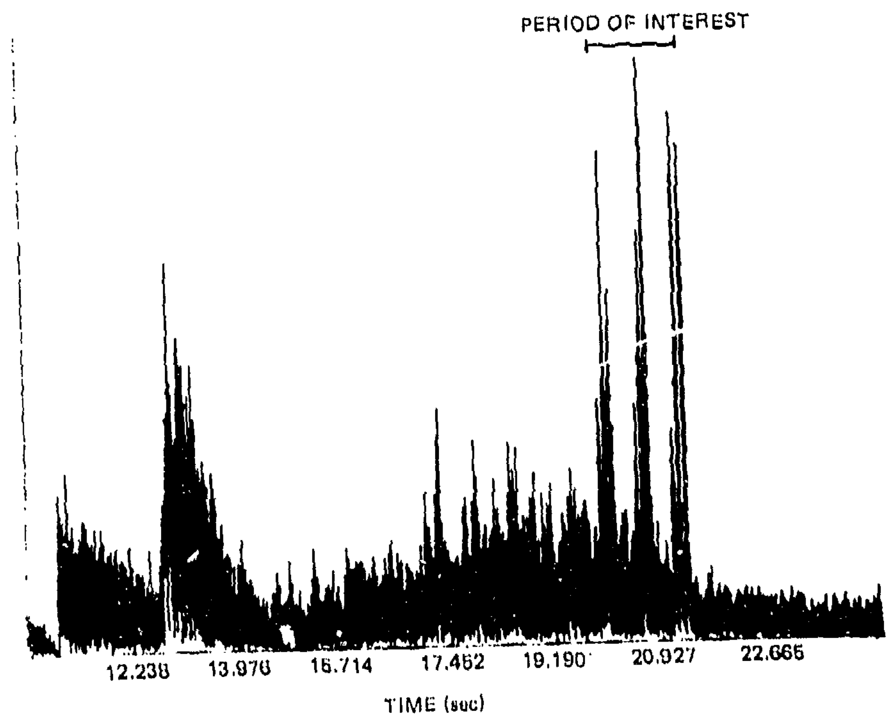

Figure 15e. RC (ping 149).

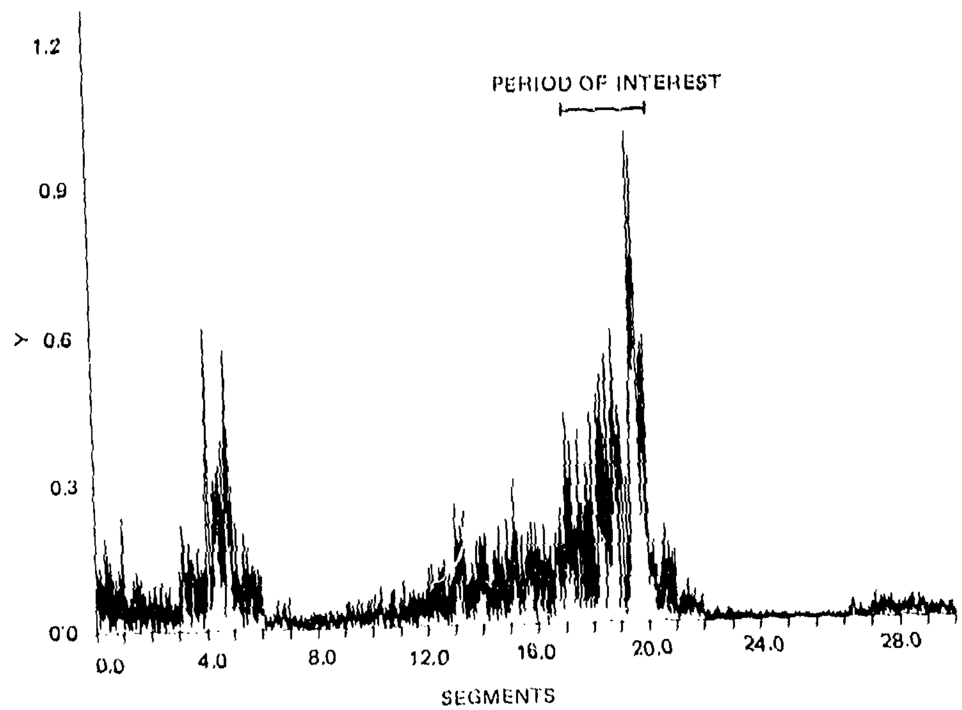

Figure 15f. EEC (ping 149).

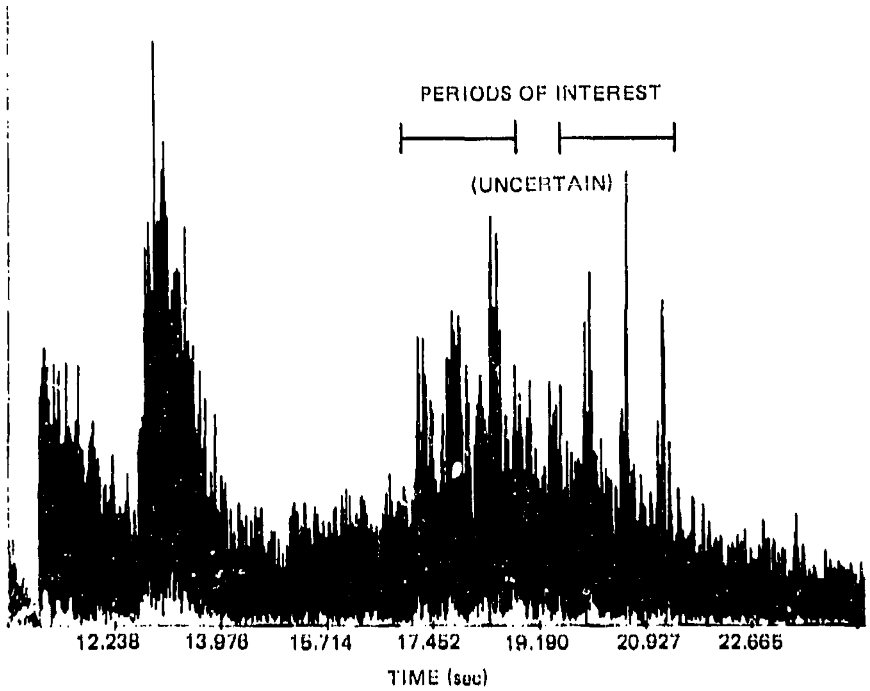

Figure 15g. RC (ping 150).

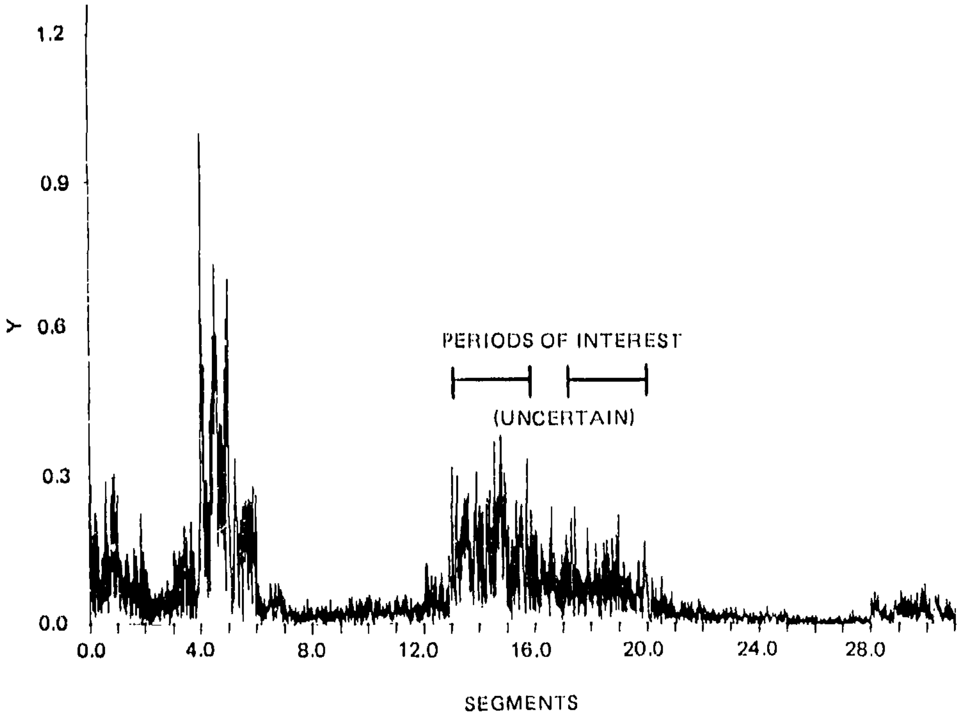

Figure 15h. EEC (ping 150).

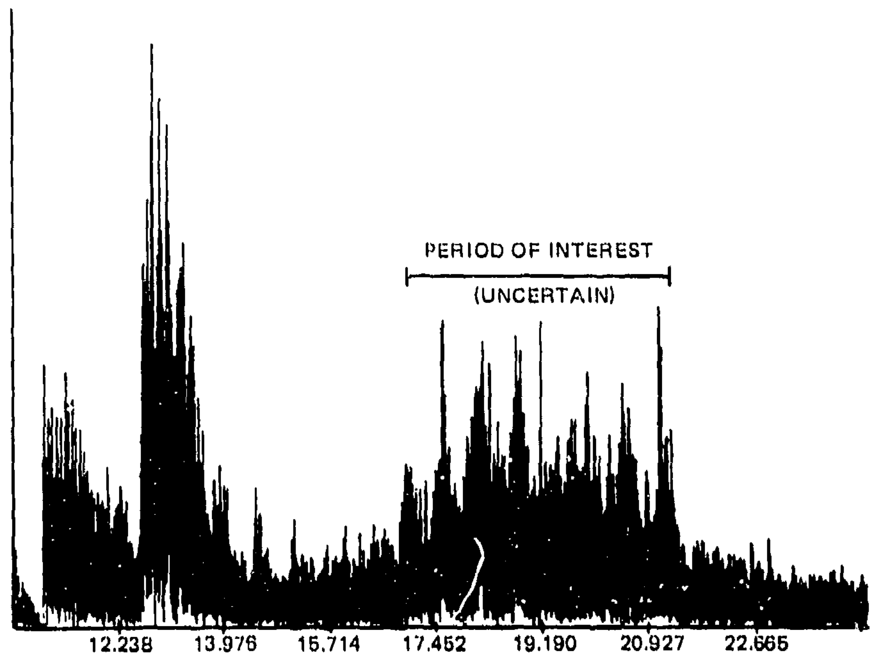

Figure 15i. RC (ping 151).

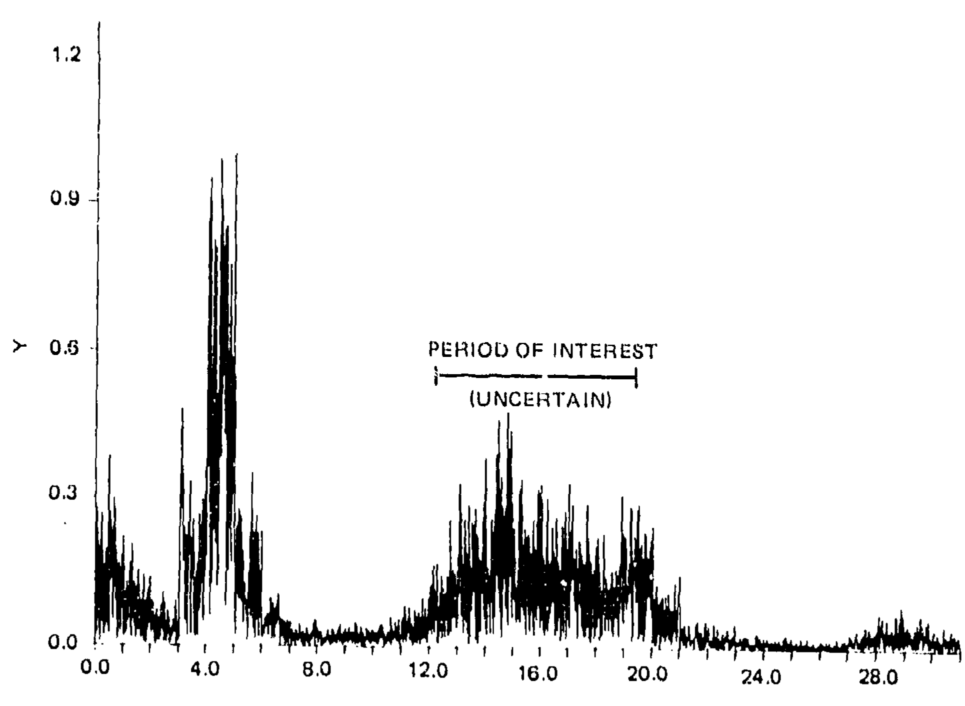

Figure 15j. EEC (ping 151).

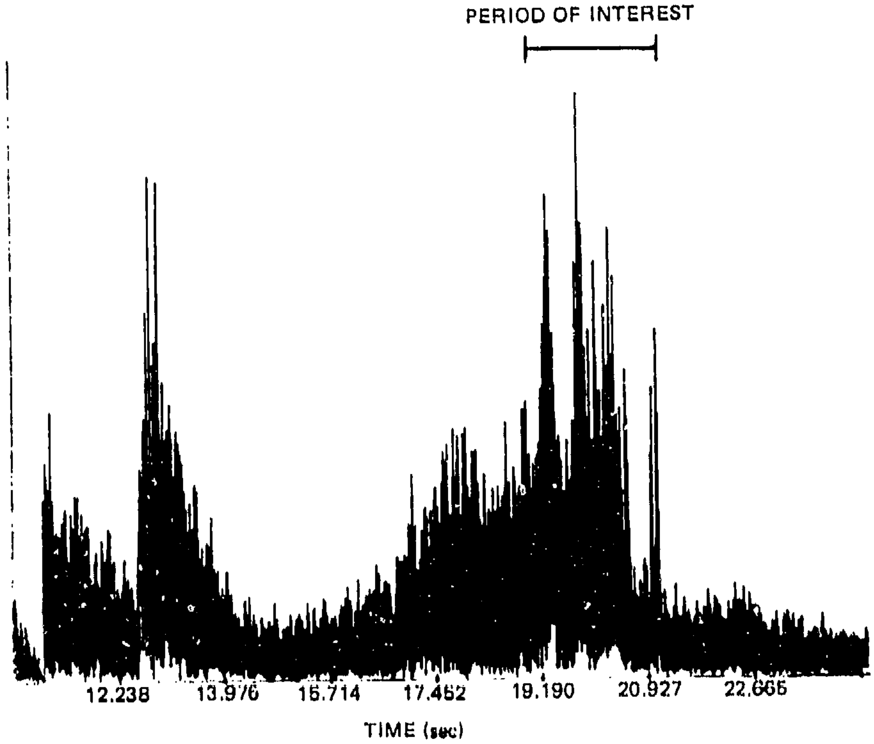

Figure 15k. RC (ping 152).

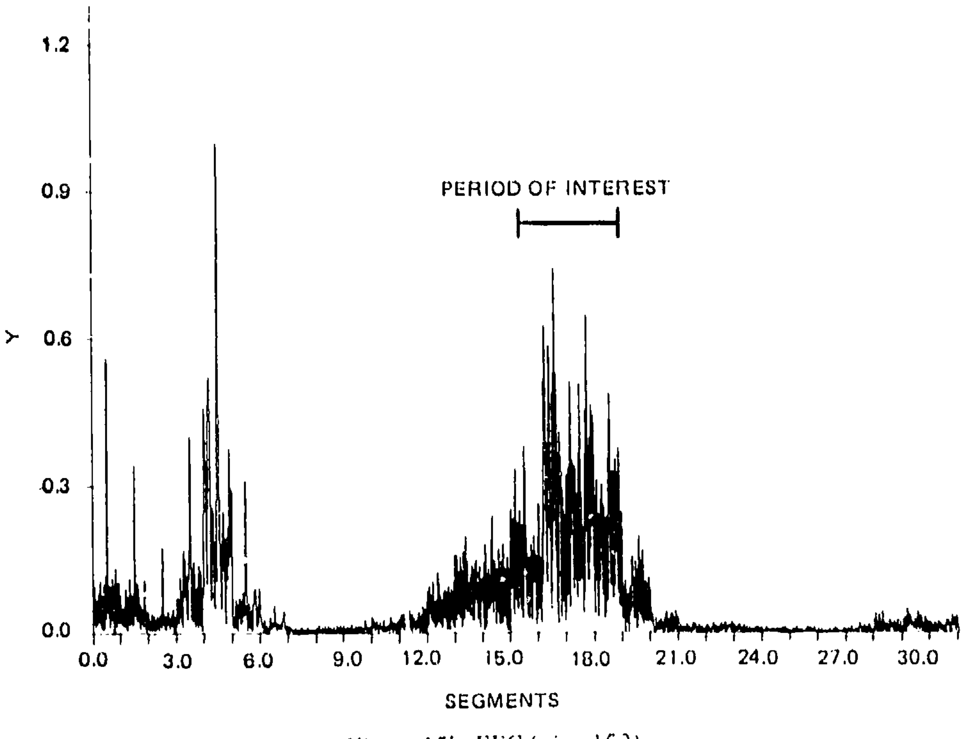

Figure 15l. EEC (ping 152).

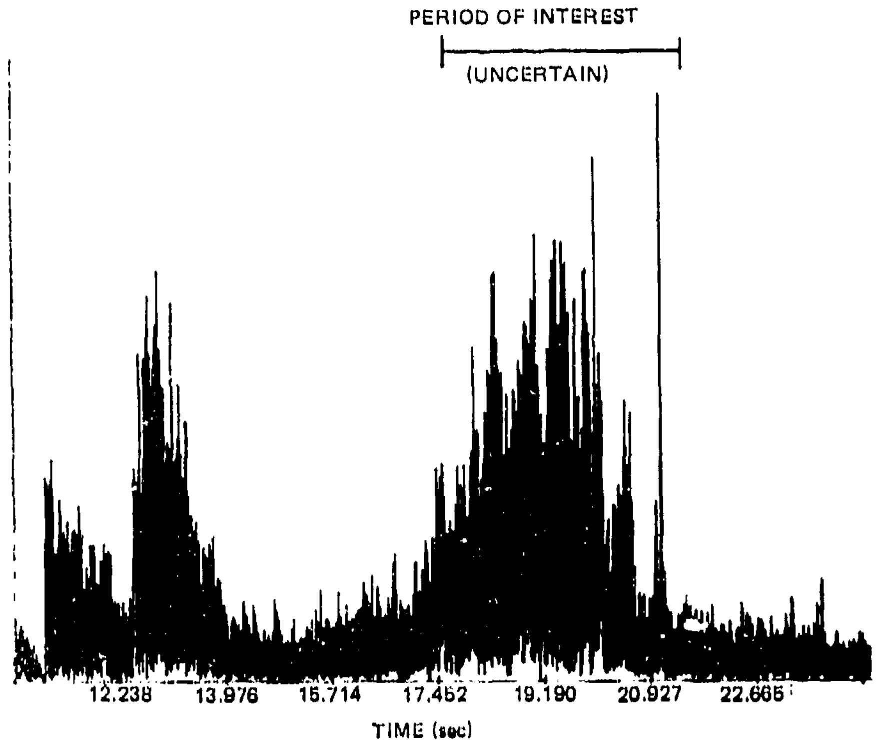

Figure 15m. RC (ping 153).

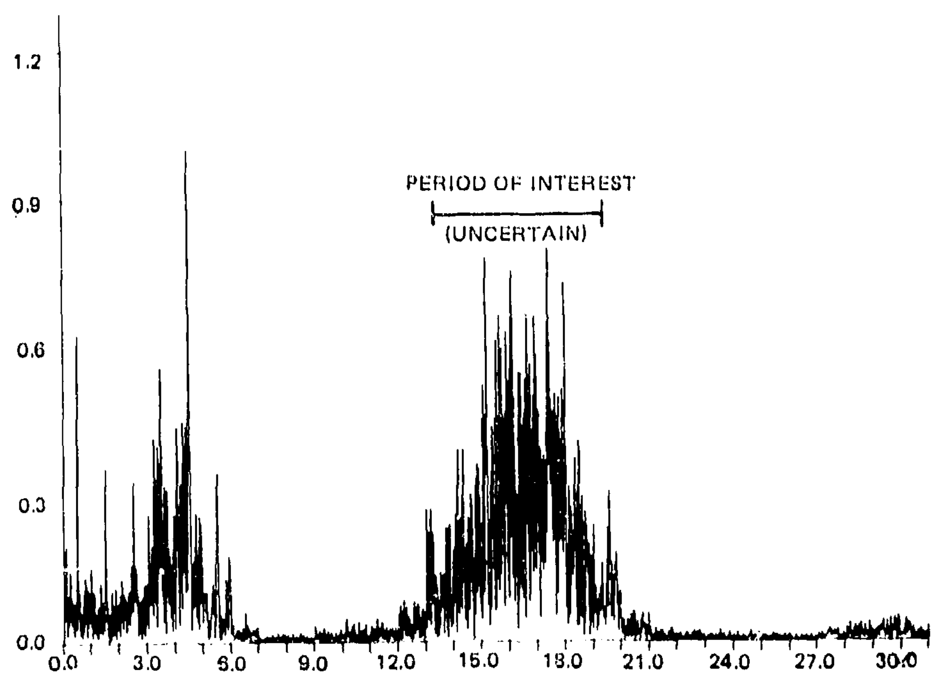

Figure 15n. EEC (ping 153).

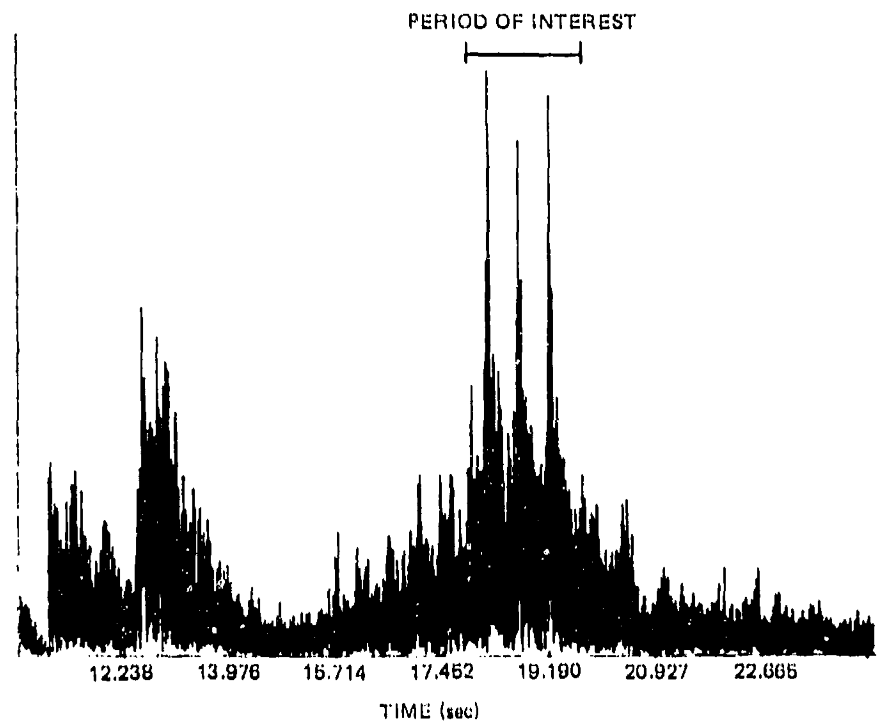

Figure 15o. RC (ping 154).

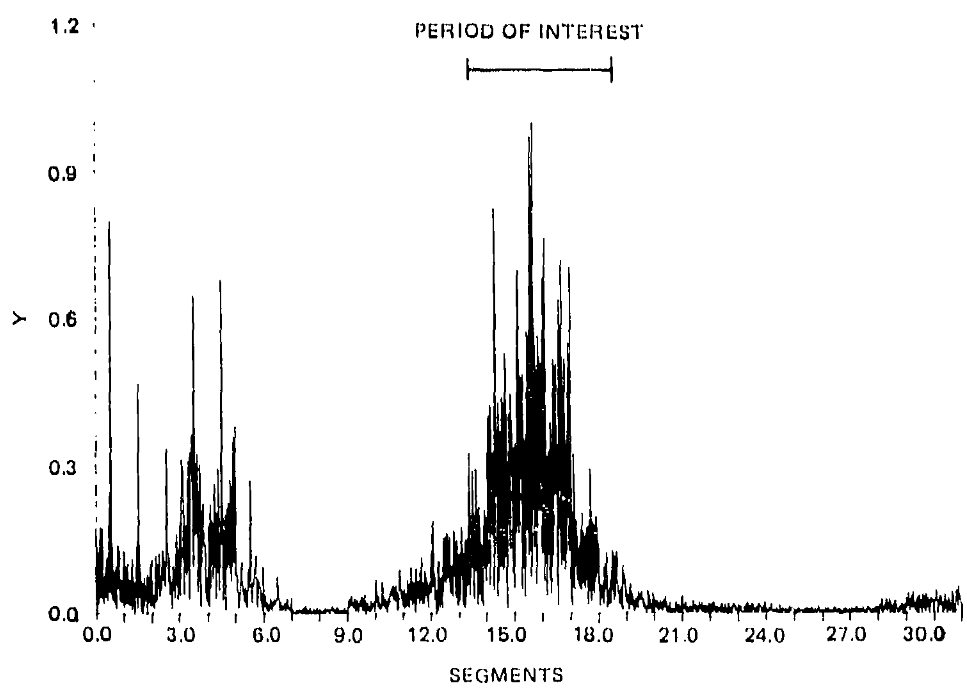

Figure 15p. EEC (ping 154).

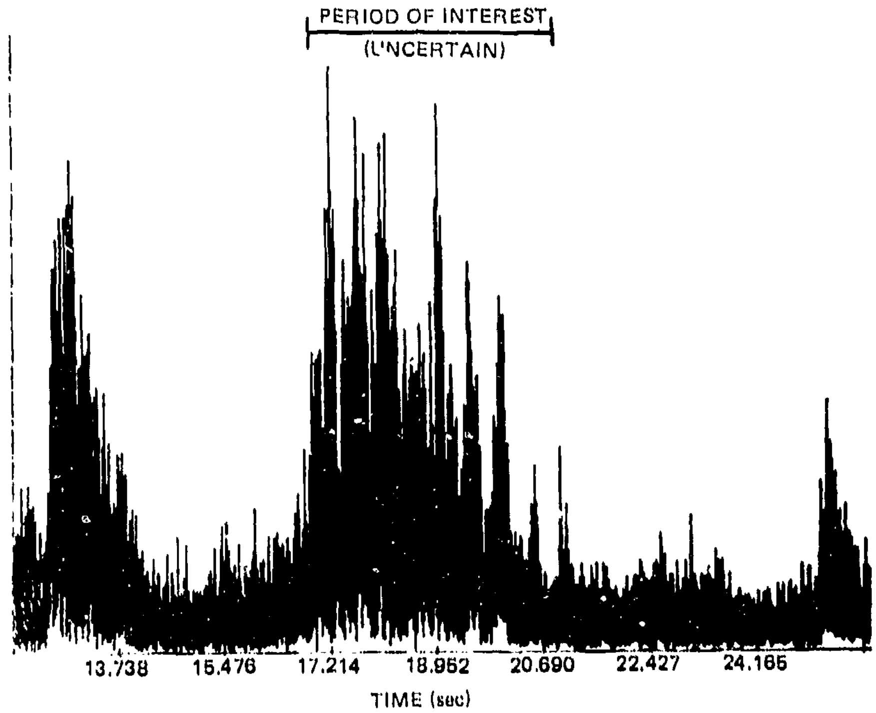

Figure 15q. RC (ping 155).

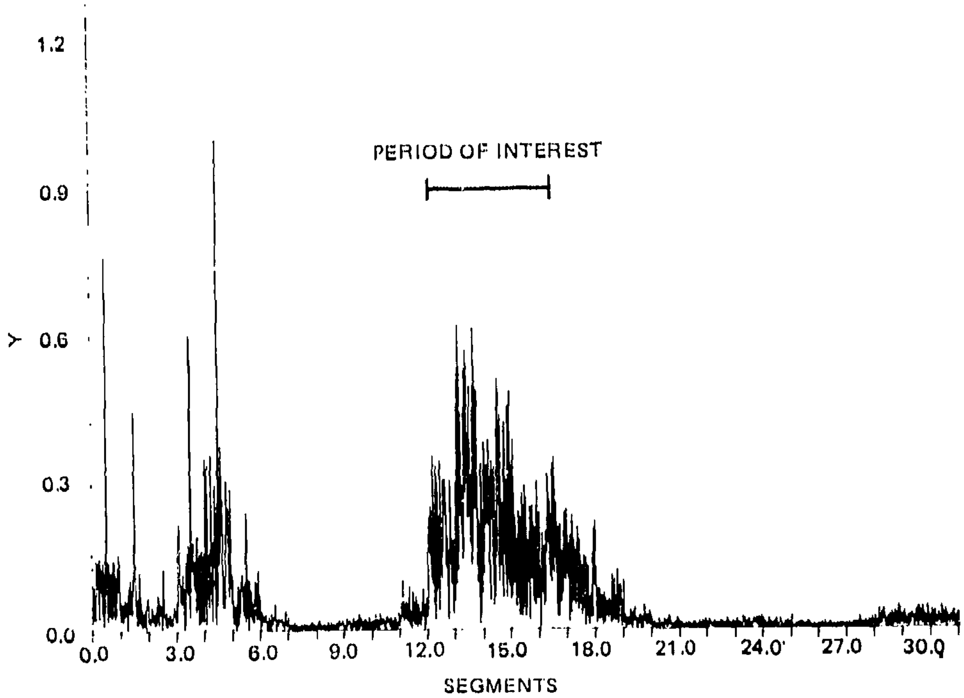

Figure 15r. EEC (ping 155).

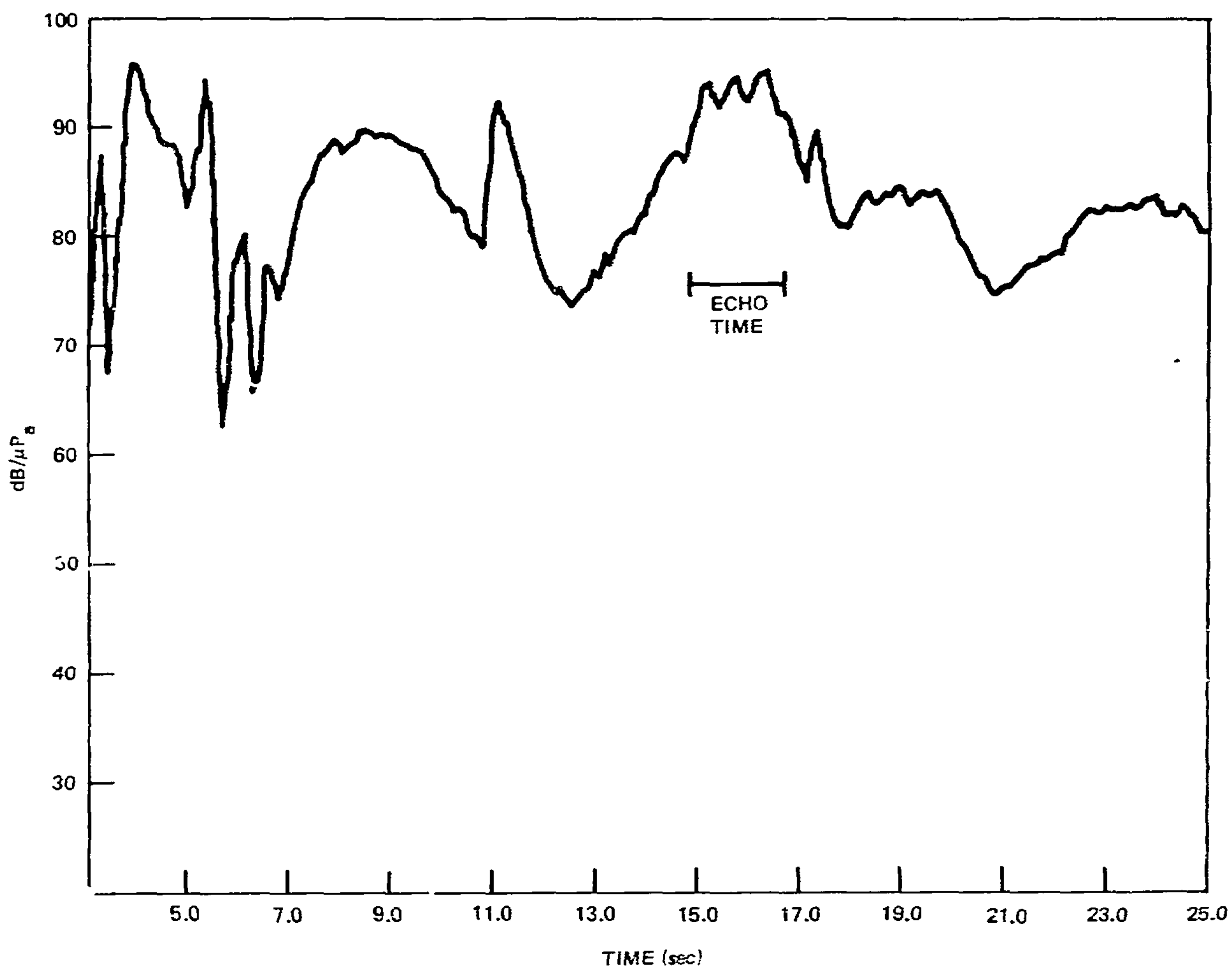

Figure 16. Reverberation time history, D/E 45°.

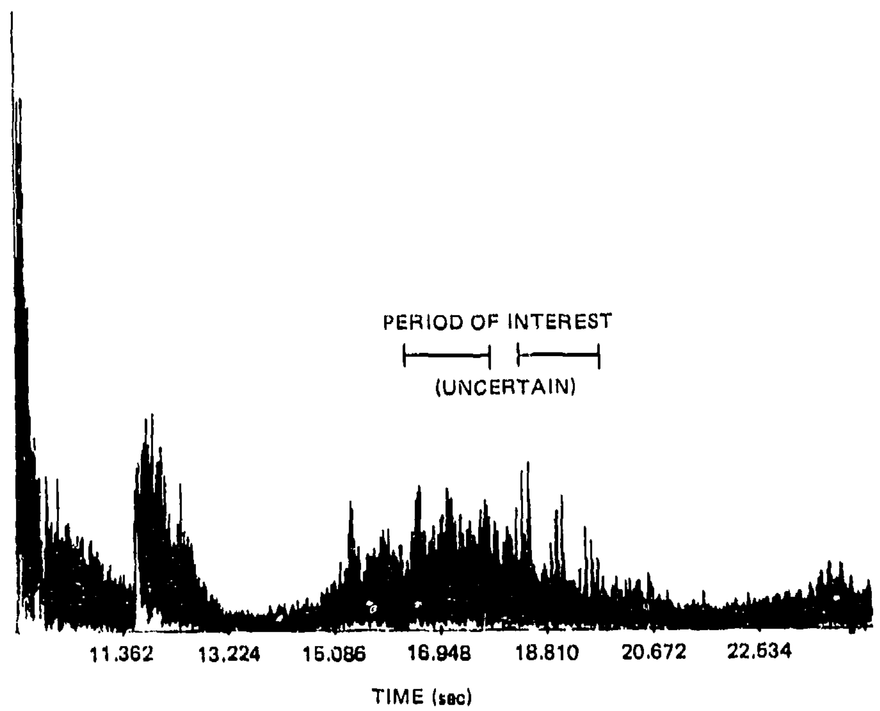

Figure 16a. RC (ping 82).

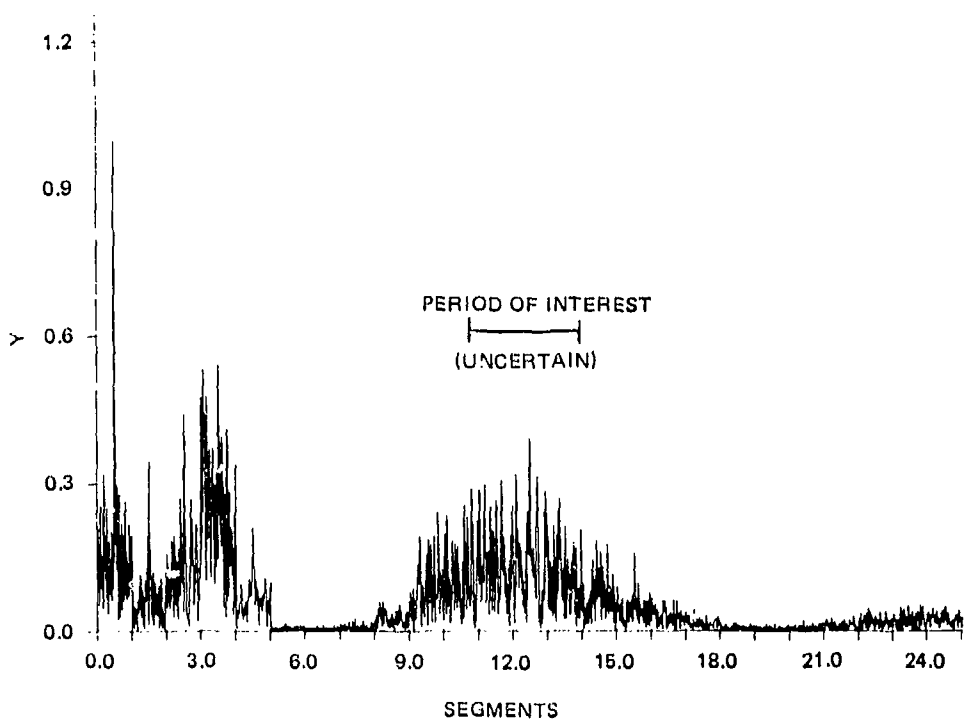

Figure 16b. EEC (ping 82).

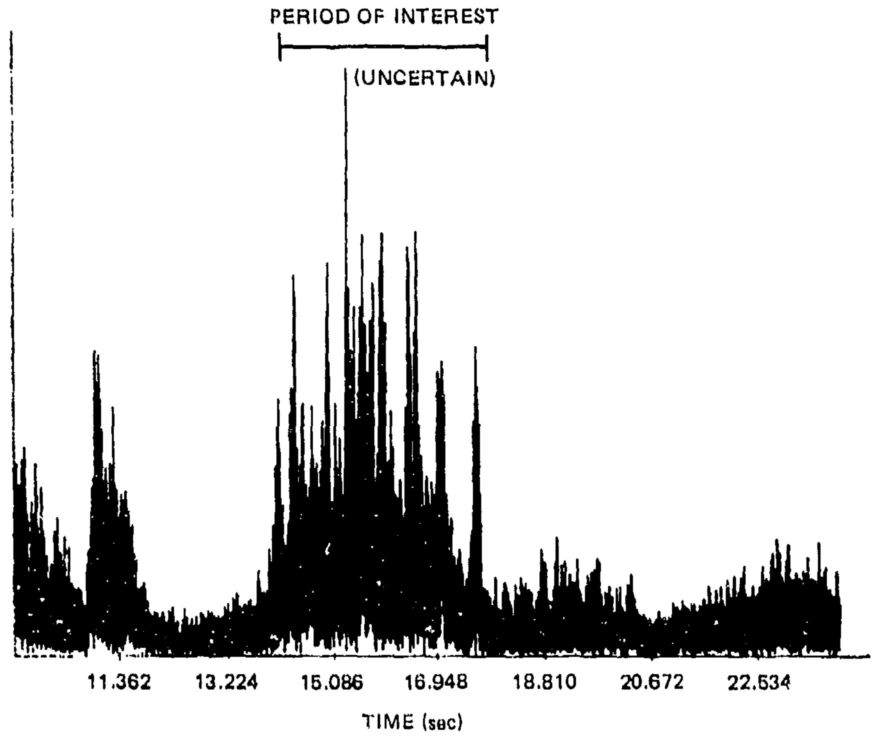

Figure 16c. RC (ping 83).

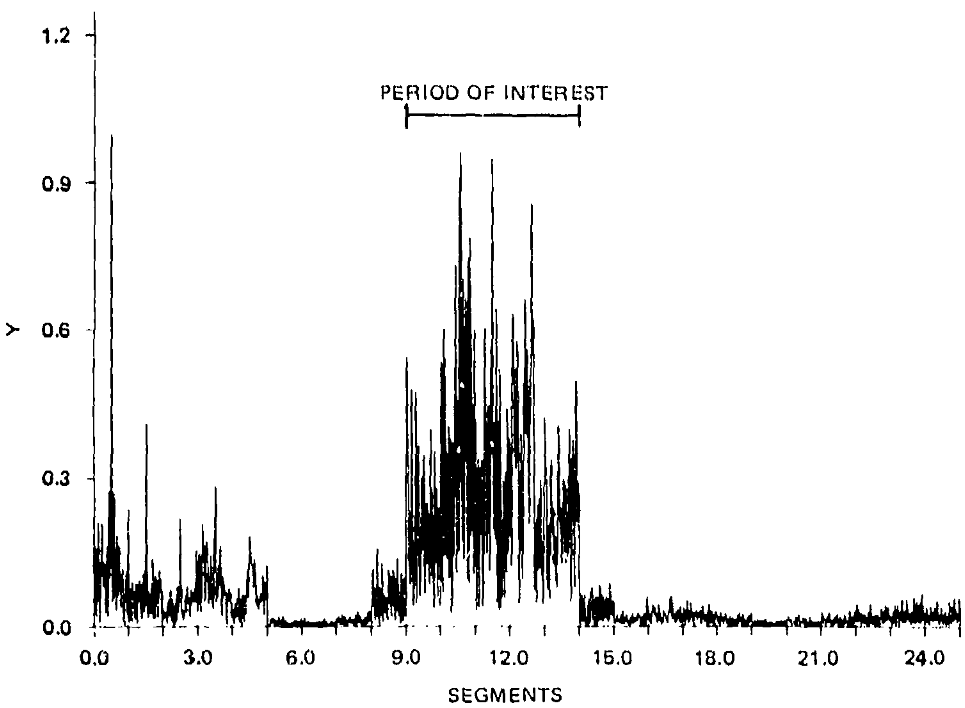

Figure 16d. EEC (ping 83)

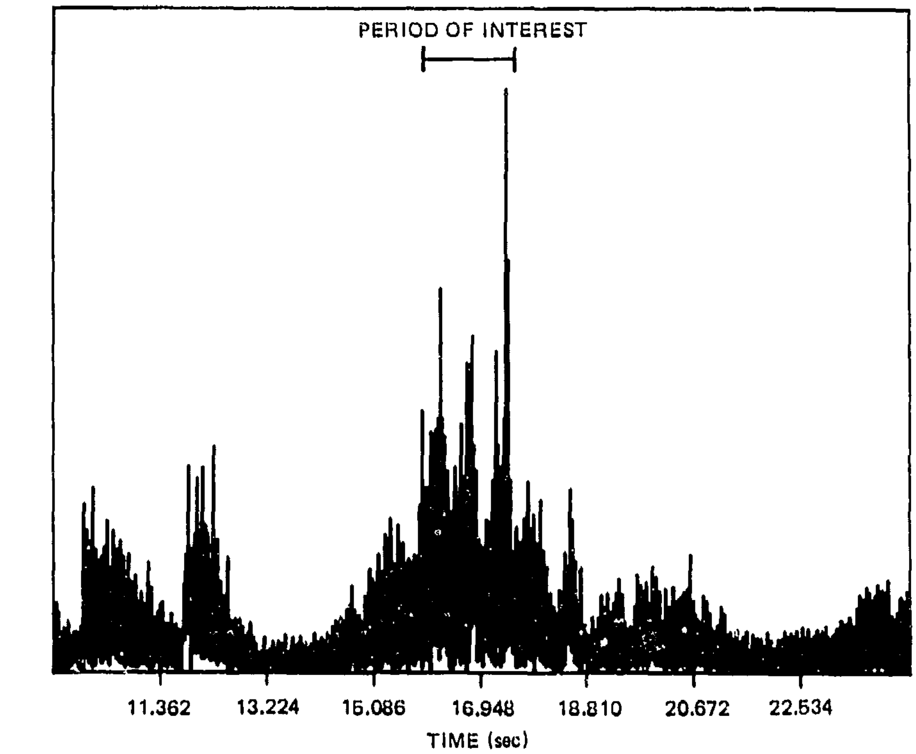

Figure 16e. RC (ping 84).

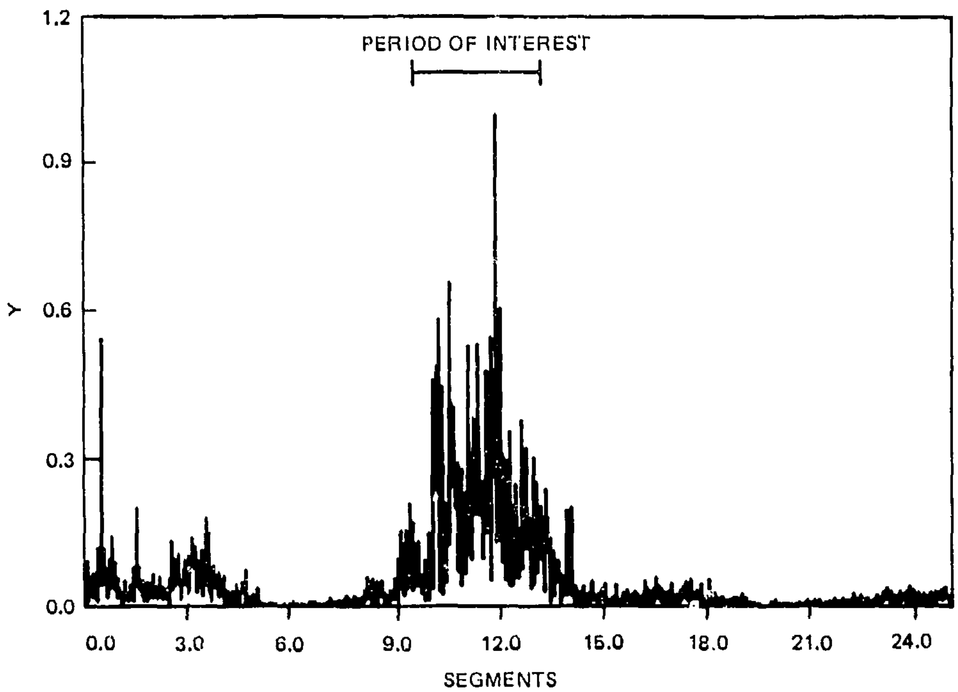

Figure 16f. EEC (ping 84).

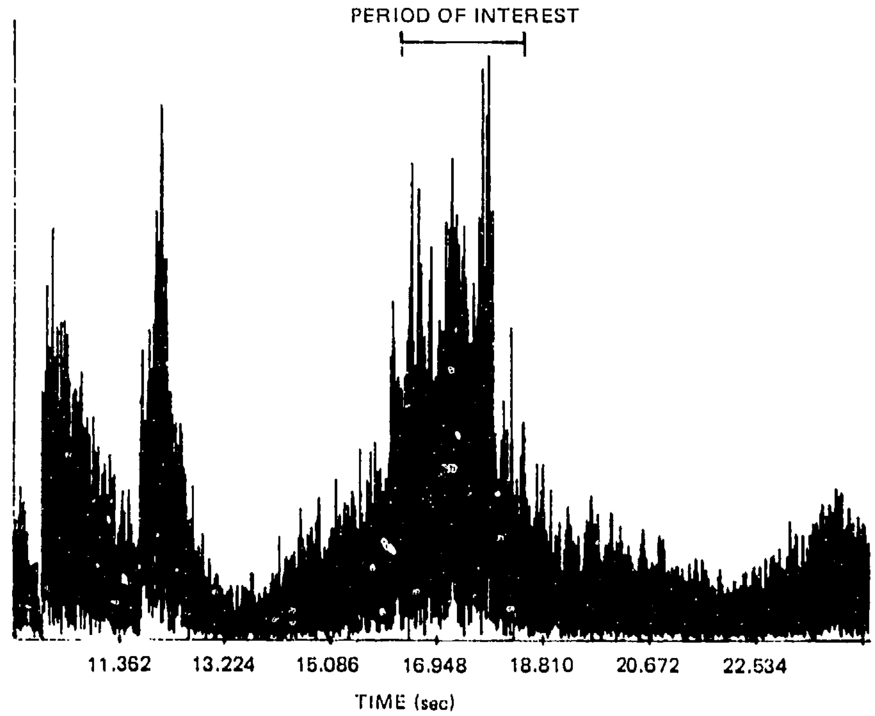

Figure 16g. RC (ping 85).

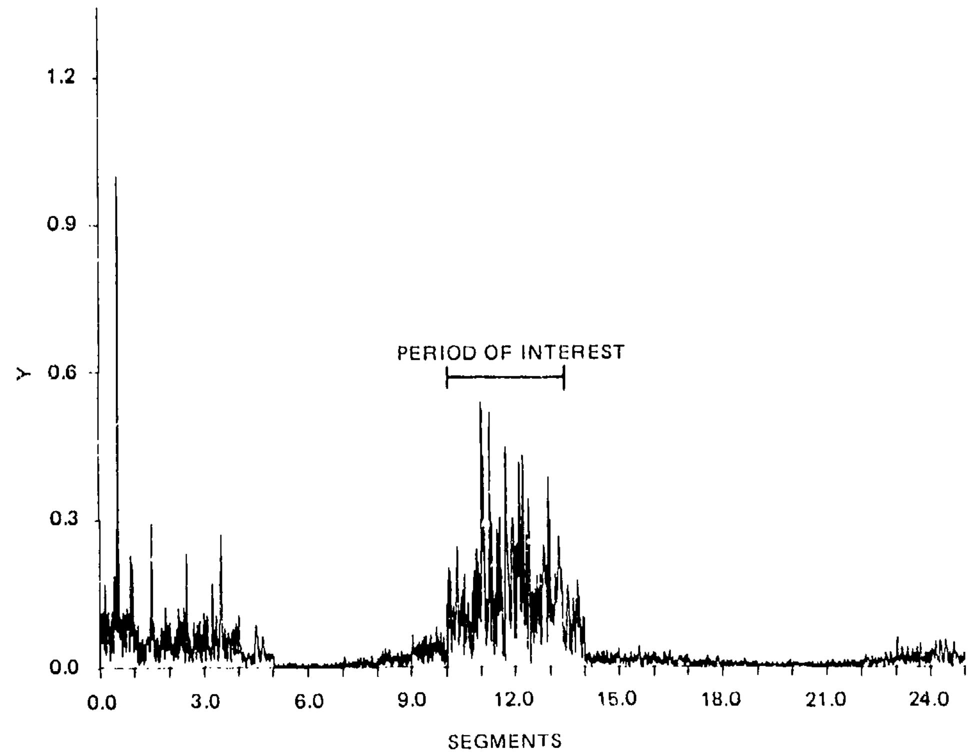

Figure 16h. EEC (ping 85).

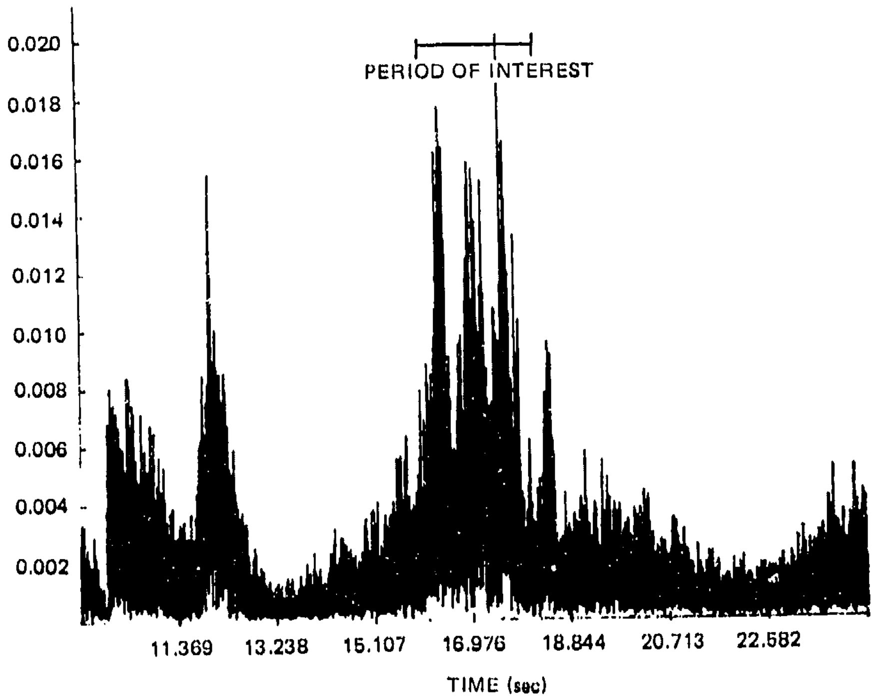

Figure 16i. RC (ping 86).

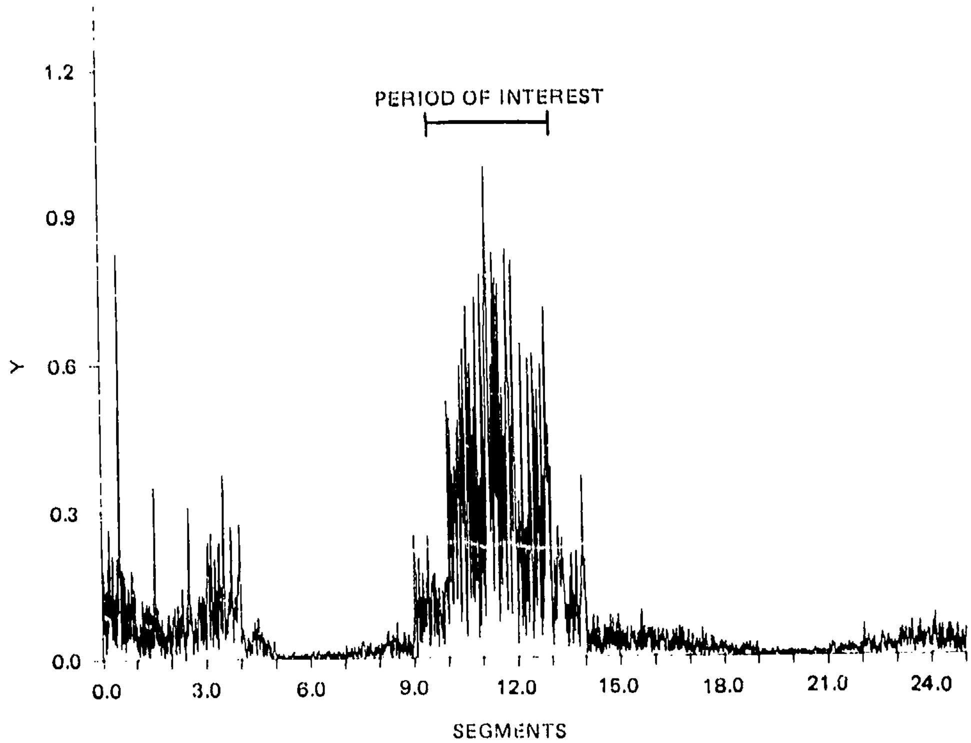

Figure 16j. EEC (ping 86).

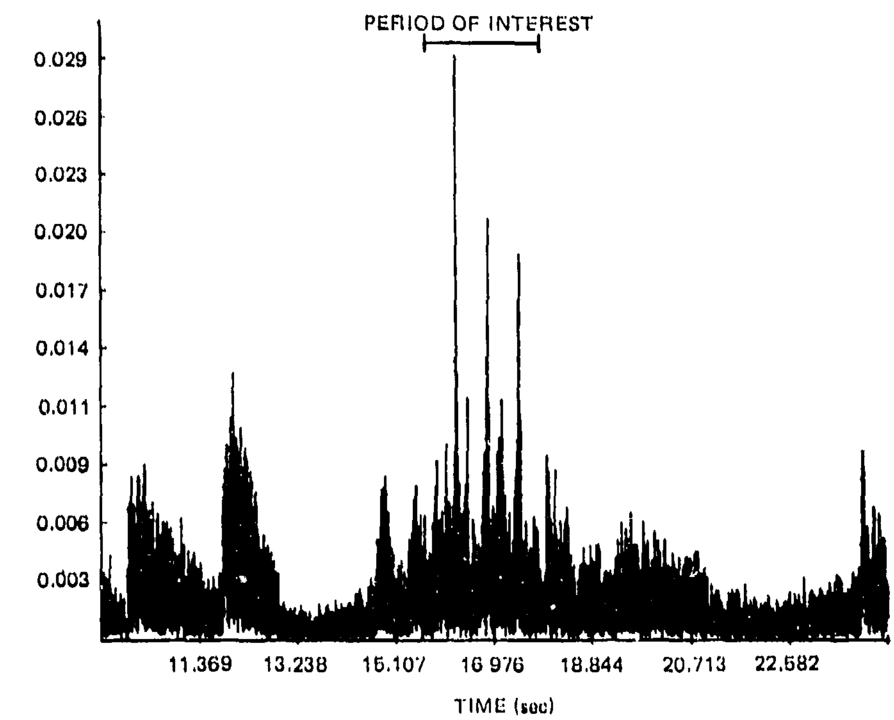

Figure 16k. RC (ping 87).

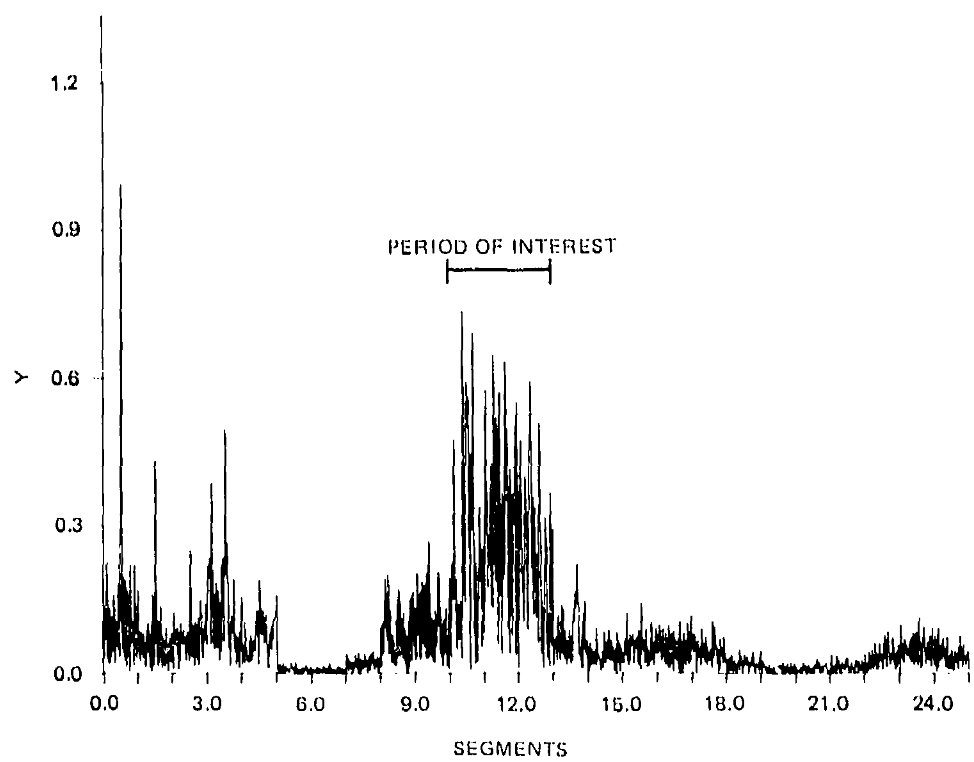

Figure 16l. EFC (ping 86).

a rather characteristic appearance (see Fig. 11, for example) not available with RC, and such a "normalization" would destroy this appearance. Further work is required on this point.

Although the data are sparse, the EEC results appear to improve with respect to RC as the range increases. Compare Fig. 11, the longest range, with Fig. 16, the shortest. This is perhaps a result of the increased multipath interference with range degrading RC.

All of the previous discussion presupposed identical input signals to (white) noise ratios as the basis for SNR comparison between EEC and RC. In the case of practical sonar comparisons, it must be pointed out that a transmission of three pulses suitable for EEC requires substantially more signal power transmission than does the single pulse necessary for RC for a comparable input echo to reverberation level, S_i. The EEC pulse train causes a three-fold increase in background reverberation for each individual returning echo. Against this loss must be measured the gain inherent in multipath recombination that is characteristic of EEC, as well as the reduction in false alarm rate.

CONCLUSIONS

Echo-Echo Correlation has a number of characteristics that distinguish it from replica correlation and which suggest that EEC may be a superior detection tool under a variety of environmental and operational situations. A summary of the characteristics is given below:

LOCATION OF TARGET RETURN

The peak echo correlation will always be found at a known or estimable location in the correlator output: at segment center for the fixed target case or within a short time span about the segment center for the moving target condition. Such *a priori* knowledge is not available for replica correlation.

PLATFORM STABILITY

Sonar platform motion will shift the output echo peak about the segment center in a possibly random manner. Without a stabilized, or motion compensated platform, the analysis of target doppler would be difficult.

MULTIPATH AND ECHO SPLITTING LOSS

EEC is relatively insensitive to multiple returns of both types provided the target is not undergoing high accelerations. Replica correlation may be severely degraded.

TARGET DOPPLER SENSITIVITY

EEC may suffer a minor loss in correlator amplitude caused by echo truncation, but is insensitive to velocity-induced frequency distortion.

PULSE TYPE SENSITIVITY

For a motion compensated platform, EEC is wholly insensitive to pulse type. As an example, doppler-distorted PRN is handled with the same filters as any for other pulse type, but the replica correlator must have a large bank of doppler-shifted replicas to handle just this case alone.

FALSE ALARMS

Since the peak return occurs about the segment center, the probability of detection is independent (within doppler constraints) of the number of samples displayed in the output. Thus, only a small portion of the output for each segment need be displayed, thereby greatly reducing the false alarm rate. Replica correlation requires that all output samples be displayed, with a much higher false alarm rate.

SNR ENHANCEMENT

Knowing the precise location of the correlator peak allows the use of Eq. (16), namely, $\bar{c}_k(\lambda) = c_k(\lambda) + c_k(-\lambda)$ where $c_k(\lambda)$ is the standard EEC output in a segment. $\bar{c}_k(\lambda)$ will have a 3 dB gain in signal-to-noise ratio over $c_k(\lambda)$.

CHARACTERISTIC APPEARANCE

Replica Correlation in a reverberation background provides distinguishable detections only in terms of amplitude above background. EEC returns, in addition, may offer a characteristic appearance that is a useful aid in detection.

REFERENCES

1. Helstrom, C.W., Statistical Theory of Signal Detection, Pergamon Press, New York, 1968, p. 13.

2. Tracor Corporation, Technical Memorandum 66-203-4, "A Comparison of the Performance of Several Signal Processors," by P.B. Brown, March 1966, pp. 39–42 and 61–65.

3. Davenport, W.B., and Root, W.L., Random Signals and Noise, McGraw Hill, New York, 1958, pp. 81–84.

4. Whalen, A.D., Detection of Signals in Noise, Academic Press, New York, 1971, pp. 102–105.

5. IT&T Corporation, Reference Data for Engineers, New York, 1965, p. 991.

6. Bendat, J.S., and Piersol, A.G., Random Data: Analysis and Measurement Procedures, Whiley-Interscience, New York, 1971, pp. 119–122.

7. Naval Ocean Systems Center, NOSC TR 228, "Replica Correlation of Linear Period Modulated (LPM) Signals," by M.D. Green, June 1978.